

Dynamics and solar wind control of the recovery of strong geomagnetic storms

O. Ahmed^{1,2}, B. Badruddin^{1*†}, M. Derouich^{1†}

^{1*}Astronomy and Space Science Department, Faculty of Science, King Abdulaziz University, Jeddah 21589, Jeddah, P.O. Box 80203, Makkah, Saudi Arabia.

²Department of Physics, Faculty of Natural and computational Sciences, Debre Tabor University, Street, Debre Tabor, P.O. Box 272, South Gondar, Ethiopia.

*Corresponding author(s). E-mail(s): badr.physamu@gmail.com;
bzahmad@kau.edu.sa;

Contributing authors:

osmanr18@ymail.com; oahmedindris@stu.kau.edu.sa;
derouichmoncef@gmail.com;

†These authors contributed equally to this work.

Abstract

In this work we have studied about the characteristics and dynamical changes during the recovery time of moderate and strong geomagnetic storms of ($Dst < -50$ nT). In our investigation of 57 storms triggered by CMEs/CIRs, we concentrated on the solar wind's influence on their decay phases. Selected storms were classified into distinct groups based on their recovery characteristics. Employing the superposed epoch analysis and best fit methods, we scrutinized several interplanetary solar wind plasma and field parameters and their various functions. The analysis encompassed various single, dual, and multiple interplanetary plasma and field parameters/functions. We determined the most representative characteristic time for the storm's recovery profile by carefully fitting an exponential curve. A correlation analysis between Dst and solar wind parameters/functions led us to isolate a coupling function ($\rho^{\frac{1}{2}}E_y$) which best described the decay rate of the ring current. It shows that electric field term (E_y) coupled with a viscous term ($\rho^{\frac{1}{2}}$) plays pivotal role in determining the recovery rate of a geomagnetic storms. Additionally, we modeled the complex patterns of Dst recovery

in relation to solar wind parameters and functions using a second-order polynomial. Remarkably, during the recovery phase, a dynamic correlation between Dst and solar wind parameters/functions was revealed. The three-parameter solar wind-magnetosphere electrodynamic coupling functions, which combines the viscous term ($\rho^{\frac{1}{2}}$) and the electric field-related function ($v^{\frac{4}{3}}B$) ($\rho^{\frac{1}{2}}v^{\frac{4}{3}}B$), significantly impacts the recovery phase of geomagnetic disturbances. Our investigation extended to the relationship between main and recovery phase durations, providing valuable insights into the solar wind's intricate control over the decay of the geomagnetic disturbances. These findings contribute significantly to advancing our comprehension of the complex relationship between solar wind dynamics and the evolution of geomagnetic disturbances.

Keywords: solar wind, Solar coronal mass ejections, geomagnetic fields, Sun-Earth interactions

1 Introduction

Coronal mass ejections (CMEs) in general are found to be the sources of major geomagnetic storms (GSs) (e.g., [Webb and Howard, 2012](#)), while corotating interaction regions (CIRs) are more commonly responsible for moderate and weak magnetic storms. However, Bz component of the interplanetary magnetic field (IMF) typically fluctuates greatly within CIRs results weak storms (e.g., [Gonzalez et al., 1999](#); [Guarnieri et al., 2006](#); [Gupta and Badruddin, 2009](#)) that require more time to recover than CMEs (e.g., see [Xie et al., 2006](#); [Patari and Guha, 2023](#), and references therein). These phenomena are extensively studied (e.g., [Jian et al., 2008](#); [Gopalswamy, 2008](#); [Yermolaev et al., 2021](#)). In recent years, the driver sources of GSs have been identified in greater detail (e.g., [Zhang et al., 2007](#); [Echer et al., 2008](#); [Richardson and Cane, 2012](#); [Yermolaev et al., 2021](#)).

Much work has been done in recent years to better understand the causes behind magnetosphere turbulence and to make better predictions before transients, primarily from the Sun threaten the magnetosphere. GSs mostly develop in two clearly distinct phases; main and recovery. The majority of previous research concentrated on the storm's main phase (e.g., [Gonzalez et al., 1994](#); [Badruddin and Falak, 2016](#); [Manu et al., 2023](#); [Ahmed et al., 2024](#)). However, relatively fewer studies were conducted to gain a thorough understanding of the post-main phase GS activity known as the storm recovery phase (e.g., [YACOB, 1964](#); [Yermolaev et al., 2012](#); [Aguado et al., 2014](#); [Choraghe et al., 2021](#)).

Geomagnetic indices were introduced decade ago (e.g., [Mayaud, 1980](#); [Saba et al., 1997](#)), and now a days scholars are using them to investigate extraterrestrial interactions with the Earth's magnetosphere, and among them Dst is the most studied geomagnetic index (e.g., [Lin, 2021](#); [Nuraeni et al., 2022](#); [Bergin et al., 2023](#); [Miteva and Samwel, 2023](#); [Ahmed et al., 2024](#)). Previous studies show solar wind-magnetosphere interactions (e.g., [Badruddin, 1998](#); [Kane and Echer, 2007](#); [Echer et al., 2008](#); [Khabarova and Yermolaev, 2008](#); [Badruddin and Singh, 2009](#)) which are the the main drivers for GS activity (e.g., [Gosling and Pizzo, 1999](#); [Wang et al., 2002](#); [Gopalswamy,](#)

2008). The relationship between GS and interplanetary (IP) plasma and field parameters solar wind (SW) speed v , plasma density ρ and IMF B_z have been studied and suggested to be strongly related with the intensity of severe GSs (e.g., [Garrett et al., 1974](#); [Mansilla, 2008](#)). The horizontal component of low latitude magnetic fields has the magnitude reduced during one to several hours during the main phase of GSs, and it can take several days to recover (e.g., [Lakhina and Tsurutani, 2018](#)). In addition to the single plasma and field parameters, derived solar wind-magnetosphere electro-dynamical CFs have also been studied (e.g., [Srivastava and Venkatakrishnan, 2004](#); [Kane, 2005](#); [Singh et al., 2006](#); [Manu et al., 2023](#)) and many of them reported that IP electric field, during southward IMF is best correlated with the geomagnetic index Dst.

Long-lasting southward IMF B_z is the primary source of severe magnetic storms (e.g., [Echer et al., 2008](#)) which increase the magnetic reconnection of energy injection into the magnetosphere (e.g., [Tsurutani and Gonzalez, 1997](#)) and the ring current enhancement results from this plasma injection (e.g., [Lakhina and Tsurutani, 2018](#)). It is made up of electrons and ions with energies ranging from about 1 – 400 KeV, primarily H^+ , O^+ (e.g., [Vallat et al., 2005](#); [Liemohn et al., 2016](#)). Strong GSs resulted from a high SW dynamic pressure amplifying the energy of the ring current in the presence of a consistent southern IMF B_z (e.g., [Rawat et al., 2010](#)). Ionospheric disturbances are more significant during the GSs recovery phase than before its onset (e.g., [Carrillo-Vargas et al., 2016](#)). Recent work by [Yan and Chao \(2022\)](#) suggested that geomagnetic activity is closely related to the role that O^+ ions play in ring current. However, H^+ is the predominant ion in the plasma sheet during the quiet-to-disturbance transition (e.g., [Denton et al., 2017](#)).

A number of studies have previously examined that the O^+ charge exchange loss rate concurrent with Dst dominates the faster first step recovery from the peak of Dst while the H^+ charge exchange loss rate controls the slower later step recovery (e.g., [Hamilton et al., 1988](#); [Daglis, 1997](#)) the superposition and resultant loss rates of O^+ loss rates are roughly linear (e.g., [Ji and Shen, 2014](#)). [Liemohn et al. \(1999\)](#) reported that convective drift loss out of the day side magneto-pause was found to be the primary mechanism removing ring current particles during the initial recovery of GSs. The flow out effect and the charge exchange-induced loss of confined particles are superposed to explain the recovery of the ring current (e.g., [Takahashi et al., 1990](#)). [Gupta and Badruddin \(2009\)](#) pointed out that, after the IP event, the high-speed stream's presence seems to have an impact on the storm's recovery. In addition to the constant loss of ring current particles due to common physical processes, magnetic reconnection IMF B_z Alfvén waves and magnetopause fields are also constantly injecting new particles into the magnetosphere's outer regions for CIR events (e.g., [Tsurutani et al., 2006](#)). Later [Raghav et al. \(2018\)](#) confirm that, Alfvén waves are responsible for the lengthy recovery period of GSs by introducing energy into the magnetosphere during the storm. [Raghav et al. \(2019\)](#) discussed that, not only weak/moderate (CIR driven) storms recovery is extended by Alfvén waves but also strong storms. [Shaikh et al. \(2019\)](#) suggested that Alfvén waves may contribute to slow recovery of storms. Physical processes such as recombination, in particular, are responsible for the sluggish

recovery of alfvén waves (e.g., Telsoni et al., 2021). According to theoretical simulations, it was observed that the injection of the ring current is influenced by both the dynamic pressure and electric field of the SW (e.g., Gopalswamy et al., 2022). Most of previous studies primarily examined individual events, limited to a particular solar cycle or specific GS intensities. However, our study takes a different approach by investigating the recovery phase time properties and dynamics of GSs across three solar cycles encompassing the years 1995 to 2022. Additionally, we analyze averaged storms originating from diverse drivers and varying intensities, by employing the superposed epoch analysis.

Convective electric field ($-vB_z$) effects on recovery time were first taken into account by (e.g., Fenrich and Luhmann, 1998). The suggestion of such CFs during the recovery phase motivates us to introduce more electric field-related functions, which are later combined with (viscus term ρ and dynamic pressure term P) (e.g., Newell et al., 2008) with different power indices ($\frac{1}{2}$, $\frac{1}{3}$). We obtained a useful representative derived function from such combination that expressed the recovery time characteristics better than individual component alone. Electric field functions paired with a viscus term best reflect the recovery time features of GSs, (also see, O’Brien and McPherron, 2000). Exponential constant (τ), which varies over time and is dependent on the minimum Dst, can be used to approximate the Dst profile (e.g., O’Brien and McPherron, 2000; Monreal MacMahon and Llop-Romero, 2008; Yermolaev et al., 2012). While anti-correlation exists for long duration recovery, $(Dst)_{\text{peak}}$ intensity is correlated with short durations (e.g., Aguado et al., 2010; Yermolaev et al., 2012; Cid et al., 2014). Badruddin et al. (2021) recently applied exponential fitting to the rate of decay time profile of Forbush decrease events. To describe the rate of Dst decay during the recovery period, we used an exponential curve fitting model.

In the present study, the recovery features of GSs have been investigated using the geomagnetic index Dst, as well as numerous IP SW parameters and their derived functions. Superposed epoch analysis and correlation analysis methods were employed, focusing on the recovery phase of geomagnetic disturbances. This study attempts to explore the fundamental dynamics and time aspects of the GS recovery profile. The goal is to identify the optimal IP SW parameter/function for controlling ring current decay during GSs, taking into account the Dst recovery time constant and morphology. Data retrieval, classification, and analysis techniques is covered in Section 2. In Section 3, the results based on superposed analysis subjected to exponential curve fitting, and the relationship of the geomagnetic index Dst with the other IP plasma and field parameters and their derivatives based on morphology and characteristic recovery time were explored. The results of our effort has been summarized and explained in section 4.

2 Observations and data analysis

In this study, we identified 57 GS events Dst ($Dst \leq -50$ nT) with specified criteria (mentioned below) measured with 1-hour resolution data from 1995 to 2022, spanning three solar cycles. We used the NSSDC OMNI¹ database to retrieve averaged hourly

¹<https://omniweb.gsfc.nasa.gov/ow.html>

geomagnetic index Dst, IP plasma, and field parameters. The storms that satisfied the following criteria were chosen:

- Although the peak intensity and duration of recovery vary among geomagnetic storm events, the recovery pattern should ideally follow an exponential curve, sharp recoveries over short time spans and extend recovery beyond the onset level are not considered.
- The smoothness of the recovery profiles is taken into account, and some zigzag-like dip structures with high amplitudes are excluded.
- Full or nearly full recovery profiles with different recovery time are considered

The majority of the chosen GS events are caused by IP CMEs, as each event was recognized from near-Earth IP CMEs² (e.g., Cane and Richardson, 2003).

In order to isolate CFs that best represents the decay of the ring current during the recovery phase of GSs, we have considered geomagnetic index Dst, IP SW parameters and their derived functions. We have retrieved two hourly averaged IMF parameters namely (IMF magnitude B (nT), the north-south component of IMF Bz (nT), and related variance represented by sigma field vector (σB (nT)), four IP plasma parameters (proton density ρ (cm^{-3}), SW speed v (kms^{-1}), pressure P (nPa) and dawn-dusk electric field E_y (mVm^{-1}) and multiple product CFs derived from combinations of viscous terms (ρ and P) coupled with electric field related functions (e.g., E_y & $v^{\frac{4}{3}}Bz$) v and IMF variance related functions (σB) [$v\sigma B$, $v^{\frac{4}{3}}Bz$, ρE_y , $\rho^{\frac{1}{2}}E_y$, $\rho^{\frac{1}{3}}E_y$, PE_y , $P^{\frac{1}{2}}E_y$, $P^{\frac{1}{3}}E_y$, $\rho v\sigma B$, $\rho^{\frac{1}{2}}v\sigma B$, $\rho^{\frac{1}{3}}v\sigma B$, $Pv\sigma B$, $P^{\frac{1}{2}}v\sigma B$, $P^{\frac{1}{3}}v\sigma B$, $\rho v^{\frac{4}{3}}Bz$, $\rho^{\frac{1}{2}}v^{\frac{4}{3}}Bz$, $\rho^{\frac{1}{3}}v^{\frac{4}{3}}Bz$, $Pv^{\frac{4}{3}}Bz$, $P^{\frac{1}{2}}v^{\frac{4}{3}}Bz$, $P^{\frac{1}{3}}v^{\frac{4}{3}}Bz$ and $\rho^{\frac{1}{2}}v^{\frac{4}{3}}B$] as explained in Section 3.

Selection of these functions, was motivated by earlier suggested CFs representing geomagnetic disturbances and possible mechanisms operating during the ring current development and decay (e.g., see, Akasofu, 1981; Gonzalez et al., 1989; Fenrich and Luhmann, 1998; Liemohn et al., 1999; Tsurutani et al., 2006; Newell et al., 2007, 2008; Boroyev and Vasiliev, 2023; Ahmed et al., 2024). Some new variants of earlier explored CFs have also been tested. We chose geomagnetic index, IP plasma, and field parameters, together with their product functions, for their potential importance to storm recovery. To model the storm's recovery profile, we divided the data into twelve groups based on the main and recovery phases of the time profiles and fitted them with the relevant equations. The source-based classification is also provided. We employed exponential curve fitting to fully understand recovery time patterns, which is described in detail on later Section 3.1. To fit our data, we used the exponential equation: $\text{Dst}(x) = (\text{Dst})_{\min} + Ae^{-(x-x_0)/\tau}$, where τ is the time constant, $(\text{Dst})_{\min}$ is its peak value. Our focus is on the time constant τ , which provides information on the rate of the storm recovery tabulated later in Table 2. Earlier studies employed the exponential decay function to represent the fast recovery phase of the storm (e.g., see, Aguado et al., 2010; Choraghe et al., 2021, and references therein). Most of earlier studies applied the exponential fit procedure to the recovery of a few selected individual storm events. However, in most cases the progress of recovery is highly fluctuating in its nature.

To facilitate our analysis and ensure a smoother recovery profile, we divided the

²<https://izw1.caltech.edu/ACE/ASC/DATA/level3/icmetable2.htm>

selected storms into groups and analyzed averaged data. Four groups are examined based on recovery period, which is measured from the storm’s peak value (Dst minimum) until its return to normal levels. The first group, labeled as r^1 , represents “very fast” recovery with a recovery time of ≤ 4 days and consists of 16 events. The second group, labeled as r^2 , denotes “fast” recovery, taking 4 – 6 days to reach the onset level, and comprises 14 events. The third group, labeled as r^3 , represents “slow” recovery, requiring 6 – 9 days to reach onset level, and consists of 13 events. The remaining 14 events are classified as r^4 , representing “very slow” recovery, taking more than 9 days to return to quiet level. The source-based classification of two groups and one special group, which accounts for intense storms ($\text{Dst} \leq -150$ nT), is also indicated in Table 1. To get a comprehensive conclusion, the remaining five main phase-based groupings are also examined and defined in the table notes of Table 2.

We obtained the average recovery profile of Dst for each group, as well as the concurrent profiles of several IP SW parameters/functions. Using the results of curve fit time constants, we examined the relationship between Dst and IP SW parameters/functions. By investigating the correlations, we gained insights into the parameters/functions that are more closely related to the temporal profiles of storm recovery. Furthermore, we explored the association between Dst and IP SW parameters/functions based on recovery morphology. By evaluating the correlation, we acquired insight into the parameters that are more related to the recovery dynamics of GSs.

3 Results and Discussion

Intense GSs are typically generated by CMEs, whereas CIRs only rarely generate strong storms. CMEs are responsible for 90% of the events that were analyzed, while CIRs are responsible for 10% of the events (see Table 1 last column) and two groups are considered from those driver based classification.

We categorized all of the selected GS events into four groups based on their recovery time, as described in Section 2. The distribution of events across the groups is as follows: 28% of events belong to the “very-fast” recovery group (r^1), 24.5% belong to the “fast” recovery group (r^2), 23% belong to the “slow” recovery group (r^3), and 24.5% belong to the “very-slow” recovery group (r^4). Additionally, we classified the selected storms into four groups based on the time it takes for the storm main phase duration. The groups are as follows: “very-fast” decrease events (d_1) with a decrease time of ≤ 8 hours, “fast” decrease events (d_2) with a decrease time of 9 – 12 hours, “slow” decrease events (d_3) with a decrease time of 13 – 22 hours, and “very-slow” decrease events (d_4) with a decrease time of ≥ 23 hours (Ahmed et al., 2024). One unique group was also selected for the analysis, as described in Section 2 and footnote of Table 1. As a result, we considered a total of 12 groups for this paper.

3.1 Fitting dynamics of characteristics time

We employed the superposed epoch approach to analyze Dst, IP SW parameters, and their functions, which were divided into three categories:

Table 1 Log of the selected GS data with Dst recovery time profiles and classification of storms based on criteria described on Section 2.

No	Recovery Start date & time(UT)	Recovery time(hrs)*	(Dst)min (nT)	Recovery group	Sources
1	1995-04-07T19:00	247	-149	r ⁴	CIR
2	1995-10-19T00:00	22	-127	r ²	CME
3	1997-01-10T10:00	16	-78	r ¹	CME
4	1997-04-22T00:00	72	-107	r ³	CME
5	1997-05-02T01:00	196	-64	r ²	CIR
6	1997-05-15T13:00	262	-115	r ²	CME
7	1997-05-27T07:00	243	-73	r ³	CME
8	1997-06-09T05:00	50	-84	r ³	CME
9	1997-09-03T23:00	109	-98	r ⁴	CME
10	1997-10-11T04:00	94	-130	r ²	CME
11	1997-11-07T05:00	150	-110	r ¹	CME
12	1998-01-07T05:00	30	-77	r ³	CME
13	1998-03-10T21:00	218	-116	r ²	CIR
14	1998-06-26T05:00	132	-101	r ²	CME
15	1998-08-06T12:00	187	-138	r ²	CME
16	1998-08-27T10:00	204	-155 ^Δ	r ⁴	CME
17	1998-09-25T08:00	120	-202 ^Δ	r ¹	CME
18	1998-11-13T22:00	108	-131	r ³	CME
19	1999-01-14T00:00	109	-112	r ³	CME
20	1999-09-23T00:00	92	-173 ^Δ	r ¹	CME
21	2000-01-11T23:00	177	-80	r ³	CIR
22	2000-04-07T01:00	138	-292 ^Δ	r ¹	CME
23	2000-07-16T01:00	90	-300 ^Δ	r ²	CME
24	2000-08-12T10:00	60	-234 ^Δ	r ¹	CME
25	2000-09-18T00:00	162	-201 ^Δ	r ¹	CME
26	2001-03-31T09:00	103	-387 ^Δ	r ¹	CME
27	2001-04-12T00:00	35	-271 ^Δ	r ¹	CME
28	2001-04-18T02:00	61	-114	r ¹	CME
29	2001-04-22T16:00	134	-102	r ³	CME
30	2001-08-17T22:00	89	-105	r ²	CME
31	2001-10-03T15:00	34	-166 ^Δ	r ¹	CME
32	2001-11-06T07:00	226	-292 ^Δ	r ²	CME
33	2001-11-24T17:00	149	-221 ^Δ	r ²	CME
34	2002-09-08T01:00	147	-181 ^Δ	r ²	CME
35	2003-11-20T22:00	170	-422 ^Δ	r ⁴	CME
36	2004-04-04T01:00	32	-117	r ²	CME
37	2004-08-30T23:00	124	-129	r ³	CME
38	2005-01-22T07:00	133	-97	r ²	CME
39	2005-05-15T09:00	311	-247 ^Δ	r ¹	CME
40	2006-12-15T08:00	85	-162 ^Δ	r ³	CME
41	2009-07-22T07:00	198	-83	r ¹	CME
42	2011-08-06T04:00	198	-115	r ¹	CME
43	2011-10-24T18:00	129	-147	r ¹	CME
44	2012-04-24T05:00	285	-120	r ⁴	CME
45	2012-07-15T19:00	283	-139	r ³	CME

No	Recovery Start date & time(UT)	Recovery time(hrs)*	(Dst)min (nT)	Recovery group	Sources
46	2012-11-14T08:00	231	-108	r ⁴	CME
47	2013-03-17T21:00	221	-132	r ³	CME
48	2013-06-01T09:00	101	-124	r ³	CIR
49	2013-06-07T03:00	31	-78	r ⁴	CME
50	2014-02-28T00:00	239	-97	r ⁴	CIR
51	2015-01-07T12:00	222	-107	r ¹	CME
52	2015-03-17T23:00	184	-234 ^Λ	r ³	CME
53	2015-06-23T05:00	276	-198 ^Λ	r ⁴	CME
54	2016-01-01T01:00	112	-116	r ³	CME
55	2016-10-13T18:00	205	-110	r ³	CME
56	2017-05-28T08:00	106	-125	r ²	CME
57	2018-08-26T07:00	211	-175 ^Λ	r ³	CME

r¹ - "very fast" recovery duration takes ≤ 4 days.

r² - "fast" recovery duration takes 4 to 6 days.

r³ - "slow" recovery duration takes 6 to 9 days.

r⁴ - "very slow" recovery duration takes ≥ 9 days.

* - Total recovery time from the (Dst)min to fully recovered.

Λ - Intense GS group for Dst ≤ -150 nT.

- A - a single IP SW parameter that includes (B, Bz, P, ρ , v, σB & Ey)
- B - Function of two IP parameters, of viscous terms (ρ , P, v terms) and electric field related terms ($v\sigma B$, PEy, $P^{\frac{1}{2}}Ey$, $P^{\frac{1}{3}}Ey$, $\rho^{\frac{1}{2}}Ey$, $\rho^{\frac{1}{3}}Ey$, ρEy , & $v^{\frac{4}{3}}Bz$)
- C - Functions of three IP SW parameters which comprises viscus (ρ , P, v terms) and electric field related terms ($v^{\frac{4}{3}}Bz\rho$, $v^{\frac{4}{3}}Bz\rho^{\frac{1}{2}}$, $v^{\frac{4}{3}}Bz\rho^{\frac{1}{3}}$, $v^{\frac{4}{3}}BzP^{\frac{1}{3}}$, $v^{\frac{4}{3}}BzP^{\frac{1}{2}}$, $v^{\frac{4}{3}}BzP$, $Pv\sigma B$, $P^{\frac{1}{2}}v\sigma B$, $P^{\frac{1}{3}}v\sigma B$, $\rho^{\frac{1}{2}}v\sigma B$, $\rho^{\frac{1}{3}}v\sigma B$, $\rho v\sigma B$, & $v^{\frac{4}{3}}B\rho^{\frac{1}{2}}$)

In addition to Dst, we have performed exponential curve fit to all parameters and functions (mentioned in class A, B & C above) and the results were tabulated in Table 2. However, for graphical presentation we have taken two representative parameters or functions from each class. To that end, IMF B and dynamic pressure P have been considered from class–A of single parameters (see, Figures 2 & 3), while $v\sigma B$ and PEy have been taken from class–B of two parameter derived CFs (see Figures 4 & 5). Three parameter derived CFs taken from class–C are $v^{\frac{4}{3}}B\rho^{\frac{1}{2}}$ & $P^{\frac{1}{3}}v\sigma B$ which have been shown in (Figures 6 & 7).

The exponential curve fit plots for the recovery profiles of each of the geomagnetic index, IP SW parameters/functions, as shown in Figures 1 through 7, are the results of superposed analysis for each group discussed in previous Sections. Figure 1 is the geomagnetic index Dst, and Figures (2 – 7) are the selected best two parameters from each class (A, B & C) represent the recovery profile with each figure has 12 panels for 12 different groups namely: the entire set of all 57 GSs d₅(top-left), "very-slow" dip group d₄ (top second column), "slow" dip group d₃ (top third column), "fast" dip group d₂ (top-right), "very-fast" dip group d₁ (second row left), groups r⁴ (second row second column), r³ (second row third column), r² (second row right), r¹ (bottom-left), ICME (bottom second column), CIR (bottom third column) and Int (bottom-right). The Dst recovery profile can be approximated by exponential time constant (τ), which

Table 2 List of τ from exponential fitting of recovery phase for geomagnetic index, IP SW parameters and their derivatives for various groupings as explained in the Sections 2 and 3

Group	$\tau(\text{Dst})$	R^2	$\tau(\text{Ey})$	R^2	$\tau(\rho^{\frac{1}{3}}v^{\frac{4}{3}}\text{Bz})$	R^2	$\tau(\text{B})$	R^2
d ₅	34.48 ± 0.68	0.99	7.22 ± 0	0.83	7.51 ± 0.47	0.87	19.35 ± 0.49	0.98
d ₄	32.89 ± 0.69	0.99	12.68 ± 0.83	0.87	8.58 ± 0.67	0.81	18.91 ± 0.61	0.96
d ₃	30.56 ± 0.57	0.99	4.45 ± 0.41	0.76	5.12 ± 0.41	0.80	15.18 ± 0.52	0.96
d ₂	17.08 ± 0.63	0.95	4.00 ± 0.80	0.40	4.03 ± 0.62	0.53	21.43 ± 0.77	0.96
d ₁	20.15 ± 0.4	0.98	2.25 ± 0.22	0.74	2.04 ± 0.18	0.78	15.13 ± 0.32	0.98
r ⁴	43.22 ± 0.54	0.98	45.14 ± 13.35	0.3	25.34 ± 5.80	0.38	21.85 ± 0.92	0.94
r ³	29.21 ± 1.13	0.95	10.21 ± 1.93	0.43	11.20 ± 1.58	0.57	24.95 ± 1.28	0.92
r ²	34.73 ± 1.13	0.97	7.44 ± 0.62	0.79	13.44 ± 1.13	0.79	15.00 ± 0.73	0.92
r ¹	17.46 ± 0.54	0.96	3.47 ± 0.50	0.56	3.32 ± 0.39	0.66	20.15 ± 0.73	0.96
ICME	34.77 ± 0.73	0.99	6.76 ± 0.50	0.83	6.81 ± 0.42	0.87	19.61 ± 0.47	0.98
CIR	29.23 ± 1.49	0.93	3.12 ± 0.57	0.44	4.64 ± 0.75	0.50	17.42 ± 1.33	0.83
Int	29.43 ± 0.62	0.99	3.16 ± 0.00	0.80	3.84 ± 0.26	0.85	16.38 ± 0.58	0.96
Group	$\tau(v\sigma\text{B})$	R^2	$\tau(\sigma\text{B})$	R^2	$\tau(\text{Bz})$	R^2	$\tau(v)$	R^2
d ₅	11.70 ± 0.43	0.95	12.71 ± 0.42	0.96	5.95 ± 0.51	0.78	1.3E ⁵ ± 1.3E ⁷	0.96
d ₄	26.06 ± 2.25	0.81	27.96 ± 2.69	0.79	13.15 ± 0.98	0.83	1.1E ⁵ ± 2.2E ⁷	0.77
d ₃	4.58 ± 0.30	0.86	8.22 ± 0.68	0.80	3.72 ± 0.27	0.83	164 ± 47	0.85
d ₂	11.58 ± 0.97	0.79	8.88 ± 0.77	0.78	4.10 ± 0.88	0.36	5.6E ⁴ ± 3.3E ⁶	0.93
d ₁	9.58 ± 0.38	0.94	9.00 ± 0.41	0.93	3.15 ± 0.36	0.67	265 ± 50	0.97
r ⁴	43.78 ± 6.05	0.73	22.27 ± 1.84	0.82	12.32 ± 1.71	0.58	543 ± 292	0.94
r ³	17.78 ± 0	0.84	8.93 ± 0.55	0.88	6.89 ± 1.14	0.49	1.8E ⁶ ± -	0.89
r ²	12.50 ± 0.91	0.84	14.05 ± 1.10	0.82	8.58 ± 0.64	0.83	52.33 ± 9.11	0.68
r ¹	5.04 ± 0.24	0.92	5.02 ± 0.33	0.86	4.05 ± 0.68	0.49	61.37 ± 5.08	0.92
ICME	10.34 ± 0	0.95	11.57 ± 0.42	0.95	8.27 ± 0.63	0.82	506 ± 215	0.96
CIR	19.10 ± 1.33	0.86	28.62 ± 3.26	0.73	3.15 ± 0.54	0.47	148 ± 9.27	0.99
Int	8.26 ± 0.34	0.94	10.86 ± 0.43	0.95	5.59 ± 0.47	0.79	71.51 ± 4.28	0.97
Group	$\tau(\rho^{\frac{1}{3}}v\sigma\text{B})$	R^2	$\tau(\rho)$	R^2	$\tau(\text{P})$	R^2	$\tau(\rho^{\frac{1}{3}}\text{Ey})$	R^2
d ₅	9.84 ± 0.29	0.97	10.88 ± 0.65	0.88	11.50 ± 0.26	0.98	7.90 ± 0.57	0.83
d ₄	19.44 ± 1.43	0.84	14.29 ± 1.85	0.62	15.14 ± 0.98	0.87	8.64 ± 0.64	0.82
d ₃	3.92 ± 0.21	0.90	12.16 ± 0.61	0.91	9.48 ± 0.39	0.94	6.11 ± 0.45	0.83
d ₂	10.41 ± 0.67	0.87	7.74 ± 0.67	0.78	10.10 ± 0.59	0.89	4.09 ± 0.64	0.51
d ₁	8.38 ± 0.25	0.97	8.85 ± 0.64	0.84	10.47 ± 0.27	0.98	2.20 ± 0.20	0.76
r ⁴	18.99 ± 1.34	0.85	14.92 ± 0.96	0.87	18.85 ± 1.26	0.87	28.61 ± 6.24	0.42
r ³	9.56 ± 0.44	0.92	9.07 ± 0.60	0.86	9.70 ± 0.24	0.98	11.00 ± 1.48	0.60
r ²	14.45 ± 0.87	0.88	11.91 ± 1.56	0.61	10.93 ± 0.73	0.86	14.11 ± 1.11	0.81
r ¹	12.60 ± 1.06	0.79	3.59 ± 0	0.66	5.28 ± 0.29	0.90	4.05 ± 0.47	0.66
ICME	8.95 ± 0.27	0.97	10.00 ± 0.61	0.88	10.59 ± 0.23	0.98	7.43 ± 0.48	0.86
CIR	30.51 ± 3.53	0.73	15.90 ± 1.26	0.82	8.13 ± 0.40	0.92	12.09 ± 2.03	0.49
Int	9.22 ± 0.31	0.96	9.25 ± 0.67	0.84	10.33 ± 0.29	0.97	4.40 ± 0.34	0.80
Group	$\tau(\rho v\sigma\text{B})$	R^2	$\tau(\text{P}^{\frac{1}{2}}\text{Ey})$	R^2	$\tau(\rho\text{Ey})$	R^2	$\tau(v^{\frac{4}{3}}\text{Bz})$	R^2
d ₅	8.07 ± 0.24	0.97	14.37 ± 0.40	0.86	8.21 ± 0.64	0.81	6.47 ± 0.48	0.83
d ₄	18.22 ± 1.67	0.77	6.62 ± 0.64	0.73	5.07 ± 0.49	0.74	12.51 ± 0.83	0.86
d ₃	3.48 ± 0.19	0.90	4.05 ± 0.22	0.90	8.63 ± 0.76	0.77	3.83 ± 0.39	0.72
d ₂	7.11 ± 0.41	0.88	3.92 ± 0.54	0.58	4.27 ± 0.38	0.76	3.97 ± 0.78	0.41
d ₁	7.02 ± 0.16	0.98	1.63 ± 0.13	0.82	2.63 ± -	0.77	2.04 ± 0.20	0.75
r ⁴	12.25 ± 0.79	0.87	15.11 ± 4.05	0.23	0.07 ± 504	0.63	42.87 ± 13.37	0.33
r ³	6.62 ± 0.19	0.97	8.83 ± 0.87	0.73	11.33 ± 1.15	0.72	10.13 ± 2.12	0.38
r ²	10.72 ± 0.62	0.89	11.91 ± 1.56	0.61	10.20 ± 0.94	0.76	13.85 ± 1.23	0.78
r ¹	9.13 ± 0.78	0.78	3.45 ± 0.27	0.80	3.13 ± 0.37	0.66	3.30 ± 0.43	0.61
ICME	7.37 ± 0.22	0.97	5.40 ± 0.36	0.85	7.45 ± 0.49	0.86	5.95 ± 0.43	0.83
CIR	20.52 ± 2.70	0.63	5.96 ± 1.03	0.46	5.38 ± 0.79	0.55	3.11 ± 0.60	0.43
Int	7.36 ± 0.25	0.96	2.55 ± 0.18	0.83	6.70 ± 0.76	0.69	2.99 ± 0.23	0.82

Group	$\tau(\mathbf{v}^{\frac{4}{3}}\mathbf{B}\rho^{\frac{1}{2}})$	\mathbf{R}^2	$\tau(\mathbf{v}^{\frac{4}{3}}\mathbf{Bz}\rho)$	\mathbf{R}^2	$\tau(\mathbf{v}^{\frac{4}{3}}\mathbf{Bz}\rho^{\frac{1}{2}})$	\mathbf{R}^2	$\tau(\mathbf{v}\sigma\mathbf{B}\rho^{\frac{1}{2}})$	\mathbf{R}^2
d ₅	15.58 ± 0.23	0.99	7.73 ± 0.60	0.81	7.67 ± 0.49	0.86	9.30 ± 0.26	0.97
d ₄	27.51 ± 1.82	0.89	0.06 ± 1402	0.62	7.07 ± 0.58	0.79	18.59 ± 1.40	0.83
d ₃	12.18 ± 0.40	0.96	7.69 ± 0.66	0.78	5.82 ± 0.46	0.80	3.74 ± 0.19	0.90
d ₂	14.93 ± 0.43	0.97	4.21 ± 0.37	0.77	4.04 ± 0.02	0.58	9.23 ± 0.56	0.87
d ₁	11.19 ± 0.18	0.99	2.60 ± 0.10	0.79	2.02 ± 0.18	0.78	7.96 ± 0.21	0.97
r ⁴	21.25 ± 1.07	0.92	0.07 ± 388	0.65	21.71 ± 4.82	0.38	16.05 ± 1.01	0.87
r ³	14.25 ± 0.41	0.97	11.53 ± 1.20	0.71	11.42 ± 1.43	0.63	8.41 ± 0.32	0.95
r ²	14.90 ± 0.46	0.97	8.24 ± 0.82	0.73	12.24 ± 0.95	0.81	13.13 ± 0.76	0.89
r ¹	11.66 ± 0.36	0.97	3.3E ⁻⁴ ± 0	0.02	3.72 ± 0.37	0.72	10.68 ± 0.88	0.80
ICME	7.37 ± 0.22	0.97	6.60 ± 0.52	0.81	6.89 ± 0.43	0.86	8.50 ± 0.25	0.97
CIR	20.52 ± 2.70	0.63	7.71 ± 0.82	0.70	5.49 ± 0.84	0.53	26.28 ± 3.00	0.71
Int	12.07 ± 0.24	0.99	5.54 ± 0.57	0.72	4.36 ± 0.33	0.83	8.70 ± 0.00	0.96
Group	$\tau(\rho^{\frac{1}{2}}\mathbf{E}\mathbf{y})$	\mathbf{R}^2	$\tau(\mathbf{P}^{\frac{1}{3}}\mathbf{E}\mathbf{y})$	\mathbf{R}^2	$\tau(\mathbf{P}^{\frac{1}{2}}\mathbf{v}^{\frac{4}{3}}\mathbf{Bz})$	\mathbf{R}^2	$\tau(\mathbf{P}^{\frac{1}{2}}\mathbf{v}\sigma\mathbf{B})$	\mathbf{R}^2
d ₅	8.24 ± 0.54	0.85	6.79 ± 0.42	0.87	3.45 ± 0.34	0.87	8.23 ± 0.26	0.96
d ₄	7.21 ± 0.56	0.81	8.64 ± 0.64	0.82	6.48 ± 0.67	0.71	14.85 ± 1.07	0.84
d ₃	6.89 ± 0.51	0.82	4.23 ± 0.26	0.87	3.52 ± 0.20	0.88	2.92 ± 0.11	0.95
d ₂	4.09 ± 0.58	0.57	3.98 ± 0.61	0.52	3.86 ± 0.52	0.60	9.43 ± 0.55	0.88
d ₁	2.16 ± 0.20	0.76	1.79 ± 0.15	0.80	1.54 ± 0.11	0.83	8.10 ± 0.22	0.97
r ⁴	25.14 ± 5.32	0.41	25.02 ± 6.63	0.31	1.08 ± 0.18	0.53	19.26 ± 1.32	0.86
r ³	11.18 ± 1.34	0.65	11.41 ± 1.82	0.51	12.05 ± 2.00	0.49	10.05 ± 0.39	0.94
r ²	13.32 ± 0.97	0.83	11.50 ± 0.99	0.78	7.25 ± 0.78	0.69	14.49 ± 0.75	0.91
r ¹	3.88 ± 0.43	0.68	3.17 ± 4.3E ⁻⁹	0.70	3.31 ± 0.23	0.84	21.36 ± 0.95	0.82
ICME	7.45 ± 0.49	0.85	6.03 ± 0.38	0.87	4.66 ± 0.29	0.87	7.71 ± 0.25	0.96
CIR	5.38 ± 0.79	0.55	4.85 ± 1.1E ⁻⁸	0.46	6.06 ± 1.09	0.44	9.80 ± 0.56	0.89
Int	5.15 ± 0.44	0.78	2.81 ± 0.00	0.83	2.50 ± 0.17	0.87	5.35 ± 0.20	0.95
Group	$\tau(\mathbf{P}\mathbf{E}\mathbf{y})$	\mathbf{R}^2	$\tau(\mathbf{P}\mathbf{v}\sigma\mathbf{B})$	\mathbf{R}^2	$\tau(\mathbf{P}^{\frac{1}{3}}\mathbf{v}^{\frac{4}{3}}\mathbf{Bz})$	\mathbf{R}^2	$\tau(\mathbf{P}^{\frac{1}{3}}\mathbf{v}\sigma\mathbf{B})$	\mathbf{R}^2
d ₅	3.48 ± 0.30	0.78	6.15 ± 0.22	0.95	6.01 ± 0.36	0.88	7.60 ± 0.24	0.96
d ₄	0.07 ± 377	0.65	9.16 ± 0.76	0.79	8.58 ± 0.67	0.81	19.44 ± 1.43	0.84
d ₃	3.73 ± 0.14	0.95	2.16 ± 0.05	0.98	3.66 ± 0.25	0.85	3.31 ± 0.15	0.93
d ₂	3.70 ± 0.29	0.81	6.58 ± 0.37	0.89	3.93 ± 0.59	0.54	10.78 ± 0.68	0.87
d ₁	1.27 ± 0.08	0.88	6.86 ± 0.16	0.98	1.67 ± 0.14	0.81	8.58 ± 0.26	0.97
r ⁴	0.84 ± 0.14	0.58	14.58 ± 1.10	0.83	19.99 ± 5.52	0.27	22.64 ± 1.71	0.84
r ³	12.06 ± 1.84	0.54	7.51 ± 0	0.96	11.52 ± 2.00	0.47	11.34 ± 0.53	0.92
r ²	1.39 ± 0	0.76	10.76 ± 0.45	0.94	10.40 ± 0.97	0.75	16.13 ± 0.93	0.89
r ¹	2.35 ± 0.12	0.91	6.01 ± 0.45	0.82	3.02 ± 0.29	0.74	16.04 ± 1.32	0.80
ICME	2.61 ± 0.22	0.79	5.95 ± 0.21	0.96	5.28 ± 0.32	0.87	8.44 ± 0.27	0.96
CIR	1.44 ± 0.15	0.73	4.69 ± 0.27	0.89	4.91 ± 0.88	0.45	12.20 ± 0.72	0.88
Int	1.85 ± 0.14	0.82	3.65 ± 0.14	0.95	2.70 ± 0.18	0.87	6.21 ± 0.24	0.95
Group	$\tau(\mathbf{P}\mathbf{v}^{\frac{4}{3}}\mathbf{Bz})$	\mathbf{R}^2						
d ₅	2.81 ± 0.23	0.80						
d ₄	0.07 ± 313	0.65						
d ₃	3.46 ± 0.13	0.95						
d ₂	3.61 ± 0.27	0.82						
d ₁	1.22 ± 0.07	0.89						
r ⁴	0.82 ± 0.13	0.63						
r ³	11.67 ± 1.89	0.50						
r ²	1.28 ± 0.13	0.76						
r ¹	2.26 ± 0.09	0.94						
ICME	2.32 ± 0.18	0.81						
CIR	1.47 ± 0.16	0.72						
Int	1.87 ± 0.13	0.85						

d₁, “very-fast” decline lasting less than 8 hours, d₂, “fast” reduction lasting 9 to 12 hours.

d₃, “slow” reduction that lasts between 13 and 22 hours.

d₄, “very-slow” decline lasting more than 23 hours, d₅, The entire data set.

Int, “intense” storms Dst ≤ −150 nT.

is dependent on the minimum Dst index and varies with time (e.g., [Monreal MacMahon and Llop-Romero, 2008](#); [Yermolaev et al., 2012](#)). We adopt exponential curve fit to describe the the ring current decay for each group. Those Figures depict time evolution plots of storm recovery profiles and fitted with an exponential curve for all the selected parameters/functions. The curve fit equation is: $y = y_0 + Ae^{-(x-x_0)/\tau}$. y_0 is the GS at its peak which is taken as zero hour for recovery phase. Our focus is on the time constant τ , which provides information on the rate of the storm recovery and shown inside each of the figures as well as tabulated in [Table 2](#). The scattered green boxes are our data points and the red line shows the best fit.

It has been reported (e.g., see, [Yermolaev et al., 2014](#); [Badrudin and Falak, 2016](#); [Pick et al., 2019](#), and references therein) that CMEs are generally identified as the primary origins of significant GSs, whereas CIRs are more frequently attributed to moderate and mild magnetic storms and that the recovery profile of ICME is smooth while that of CIR recovery fluctuates which is consistent with our result shown in [Figure 1](#). [Bothmer and Schwenn \(1995\)](#); [Borovsky and Denton \(2006\)](#); [Mustajab and Badruddin \(2011\)](#) reported that strong GSs with persistent IMF Bz variations are facilitated by CMEs. On the other hand, CIRs are related to milder and more moderate storms and exhibit significant Bz fluctuations. This observation is in line with the results of our finding.

The recovery phase of GS has two steps: faster first step and slower second step (e.g., [Takahashi et al., 1990](#); [Daglis, 1997](#); [Monreal MacMahon and Llop-Romero, 2011](#)). From the time characteristics of group d₂, $(Dst)_{\min} = -102$ nT, it is evident that it recovers within 17 hours. It indicates the correlation between storm intensity and recovery duration. Our result shows slower recovery duration than previous studies (e.g., [Burton et al., 1975](#)) and ([Dasso et al., 2002](#)), who reported 7.7 and 14 ± 4 hours, respectively. Therefore, more intense storms relatively takes longer duration to return its onset level. In addition to intensity of storms, the main phase duration has direct relationship with the recovery time. The longer storm main phase takes longer duration to recover from disturbance. Storms with short main phase durations shows in general two stages of recovery: a rapid first step, which takes about 30 hours for groups of d₁, d₂ and r¹, followed by a gradual second step recovery. From this results we can deduce that the ring current decays faster for storms with short main phase durations in general and it decays quickly for one day followed by slow long-lasting second-step recovery. On the other hand, storms with longer main phase duration show one step very slow steady recovery.

In the same manner as [Figure 1](#), [Figure 2](#) shows exponential decay of single parameter IMF magnitude B recovery profile with the quickest and smoothest recovery group r² and a time constant of 15 hours. In contrast, r⁴ exhibits a slow and uneven distribution with a characteristic time of 22 hours (see, [Figure 2](#)). The decay recovery dynamics on average take one day steep/sharp recovery which takes shorter duration than Dst. [Figure 3](#) shows dynamic pressure (P) which follows similar decay dynamics with IMF B, takes very short recovery duration $\simeq 12$ hours for r¹ and around one day for other groups. P has been fully recovered during 32% of the first step ring current decay. If the peak of P coincides with Dst minimum, it returns to quiet level with in the initial step of ring current decay, implies that the effect of P on the recovery of storms is

only for few hours. Notably, the P effect on the ring current decay of magnetic storms are neglected.

Figure 4 is a dual parameter CF ($v\sigma B/1000$) which shows similar recovery profile with P. It takes (5 – 44) hours to recover for fast and slow groups as (d_3 & r^4) respectively. Figure 5 is the dual parameter CF (PE_y) which shows similar dynamics with $v\sigma B/1000$. Figure 6 is triple parameter CF ($P^{\frac{1}{3}}v\sigma B/1000$) which shows similar recovery morphology with $v\sigma B/1000$. In general, Figures (4 & 6) shows that the turbulent Sigma IMF vector (σB) combined with IP SW speed (v) and P which signifies the level of fluctuations/turbulence during recovery phase of those structures. Especially, Figure 4 which has a 1:1 combination of Sigma IMF vector (σB) and v gives valuable information about the turbulence behavior storms during recovery period. Explicitly, intense GSs fluctuate for short time and less intense storms continue their recovery with turbulence for longer periods. Storms triggered by CME (where its intensity is almost double to CIR) is recovered during 50% of CIR recovery period. From this result we can suggest that during recovery of very intense storms as group 'Int' ($Dst \leq -150$ nT) only the first initial phase (28%) of recovery period has perturbation as seen from Figures 1 and 4. Intense magnetic storms are driven by CMEs with the long-duration south-ward IMF component B_z (Gonzalez et al., 1999; Echer et al., 2008). From our finding we observed that, the recovery characteristics of CF $v\sigma B$, for CME and CIR groups together with the same groups of Dst , CIR storms remain with fluctuations for the long period of time, which is supported by earlier studies (e.g., Guarnieri et al., 2006; Mustajab and Badruddin, 2011).

Figure 7 a triple parameter CF ($v^{\frac{4}{3}}B\rho^{\frac{1}{2}}/1000$) is a combination of viscous term ρ and electric field related function $v^{\frac{4}{3}}B$, shows exponential decay recovery dynamics which returns to quiet level earlier than Dst . From all IP SW parameters/functions, single parameters (Figures 2 & 3), dual parameter CFs (Figures 4 & 5) and triple parameter CFs (Figures 6 & 7) the CME driven storms recovery duration are shorter than the CIRs in (B , P and $v^{\frac{4}{3}}B\rho^{\frac{1}{2}}/1000$), where as for the rest CIR triggered storms recovered fast.

In addition to the displayed seven figures, we have analyzed the rest 22 IP SW parameters/functions, similarly with the same exponential function and their recovery characteristic follows either decay/growth and all implying values are tabulated in Table 2. Here we have present parameters which represent best recovery fits from each class (A, B & C) as (single, dual & triple functions) classifications respectively. We used derived CFs from the previous works (e.g., Newell et al., 2007; Ahmed et al., 2024) and used other functions to test their correlations with the recovery characteristics and morphology of GSs. In this work we used combinations of viscous term (ρ) and dynamic pressure term (P) with different power indices (1 , $\frac{1}{2}$ & $\frac{1}{3}$) combined with electric field related functions (IP dawn-dusk electric field $-vB_z$ and terrestrial electric field vB) which are also functions of IP SW speed v with different powers (1 , $\frac{4}{3}$) and IMF (magnitude B , north-south component B_z & Sigma vector σB which shows turbulence). Such CFs are important to get information not only in the main phase of GSs, but also for the recovery phases of GSs. Our finding confirms that, the derived electro-dynamical SW-magnetosphere CFs of viscous term (ρ) with electric field related functions are very important indicators of recovery phase of GSs. As we can see from

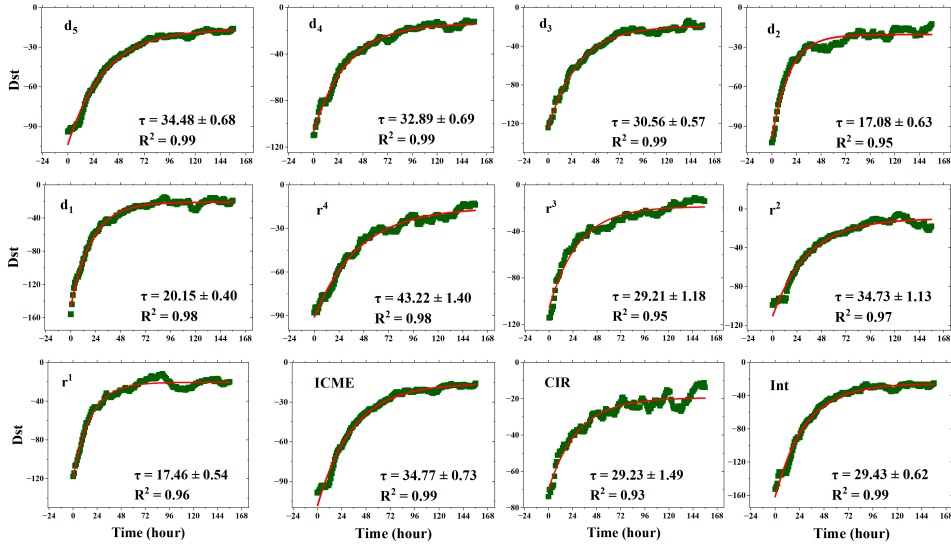


Fig. 1 shows the scatter plot with exponential fit ($y = y_0 + Ae^{-(x-x_0)/\tau}$) to the recovery phase of superposed epoch result of Dst (nT); all 57 GSs d_5 (top-left), “very-slow” dip group d_4 (top second column), “slow” dip group d_3 (top third column), “fast” dip group d_2 (top-right), “very-fast” dip group d_1 (second row right), groups r^4 (second row second column), r^3 (second row third column), r^2 (second row right), r^1 (bottom-first column), CME (bottom second column), CIR (bottom third column) and Int (bottom right). The beginning of the storm recovery is represented by zero hour in superposed charts. The red colored line shows the model curve that best depicts how our data should be fitted, while the green colored boxes represents the Dst values.

Table 2 derived functions PEy and $Pv^{\frac{4}{3}}Bz$ are the two fastest recovered parameters/-functions whereas IP SW speed v and IMF B show slow recovery. Even velocity didn’t recover fully with in our considered time intervals.

3.2 Relation between Dst and IP SW parameters recovery time constants

The impact of different SW parameters on the generation of GSs has been investigated in many previous studies, (e.g., Richardson et al., 2007; Tsurutani et al., 1992). Figure (8) show scatter error bar plots and linear regression analyses depicting the relationships between Dst and numerous IP SW parameters and product CFs. These visualizations were generated based on the recovery time constant (τ) derived from the superposed epoch analysis (see Table 2). The data points are represented by red boxes, accompanied by green bars denoting errors, and the blue lines indicate the linear fit model.

Figure 8 depicts the best-two IP SW plasma and field parameters/functions for each class (single, double, and triple) as explained in Section 3.1. Six panels are shown (the north-south component of IMF Bz and IP proton density ρ) selected as best-two

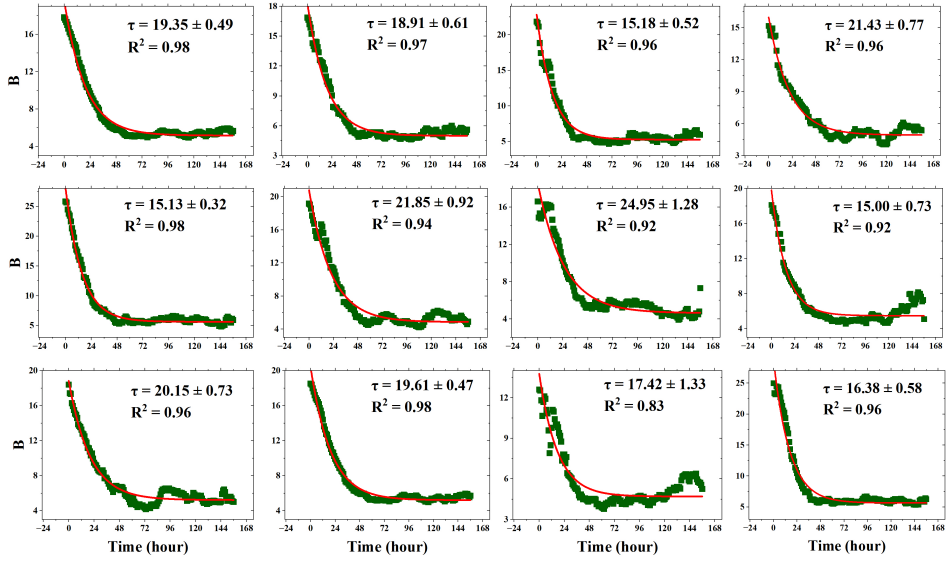


Fig. 2 Exponential fit to IMF (B) decay profile during recovery phase on respective groups adopted from Figure 1

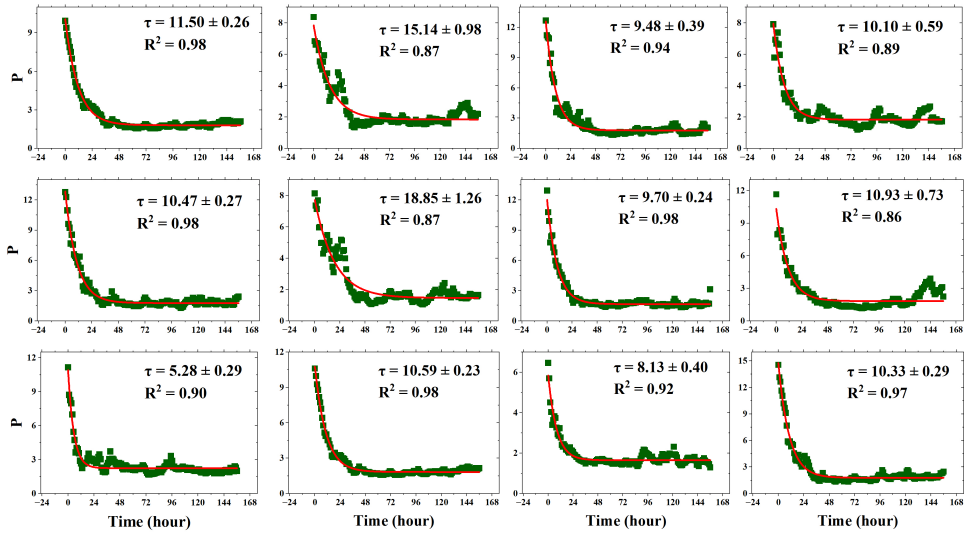


Fig. 3 Exponential fit to dynamic pressure (P) decay profile during recovery phase on respective groups adopted from Figure 1

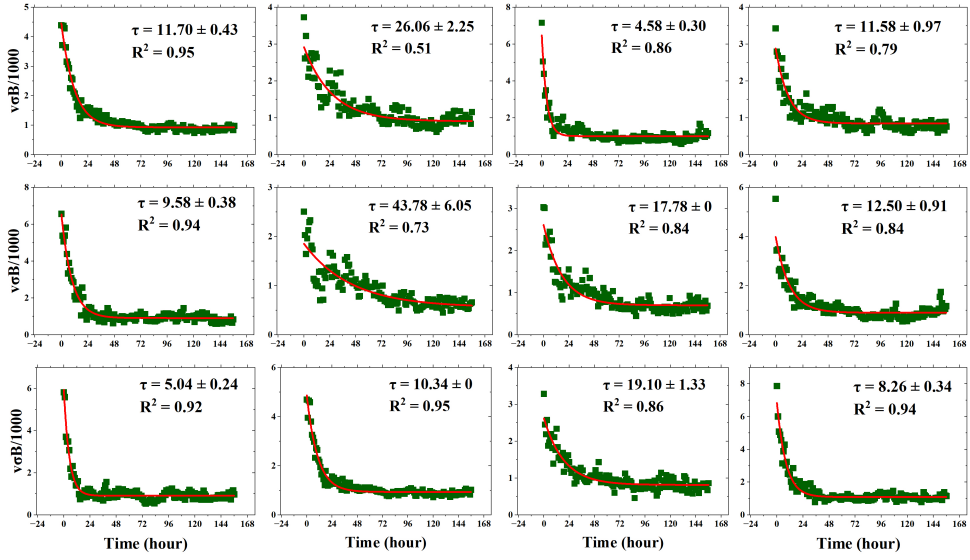


Fig. 4 Exponential fit to CF ($v\sigma B$) decay profile during recovery phase on respective groups adopted from Figure 1

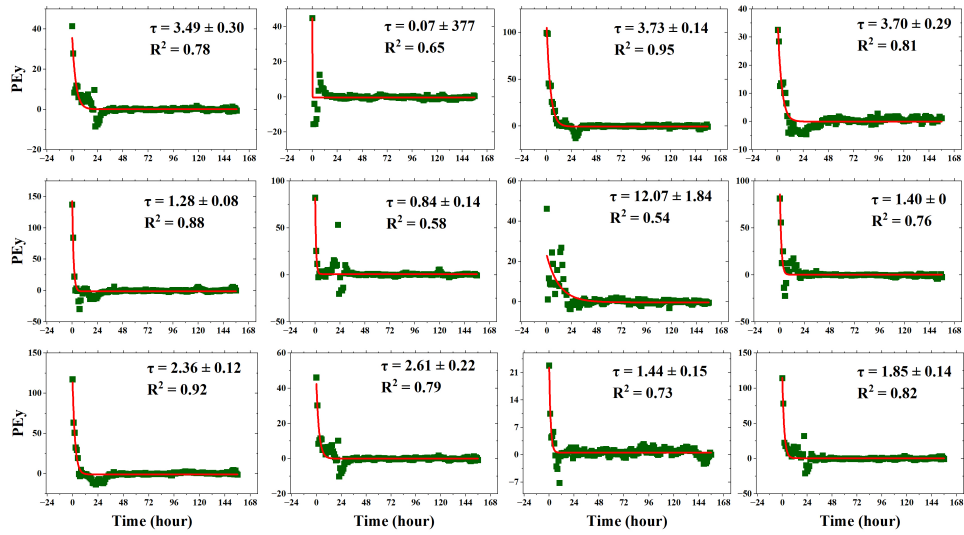


Fig. 5 Exponential fit to CF (PEy) decay profile during recovery phase on respective groups adopted from Figure 1

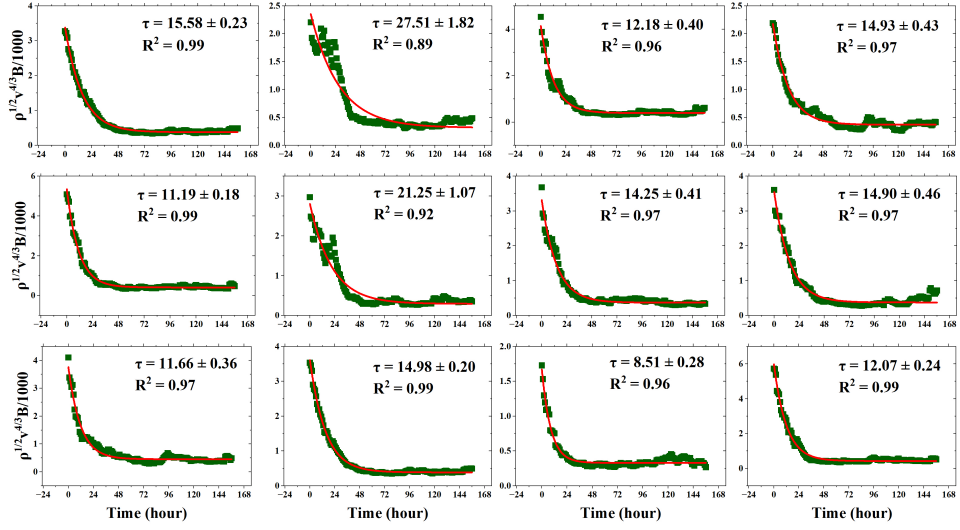


Fig. 6 Exponential fit to CF ($P^{\frac{1}{3}} v \sigma B$) decay profile during recovery phase on respective groups adopted from Figure 1

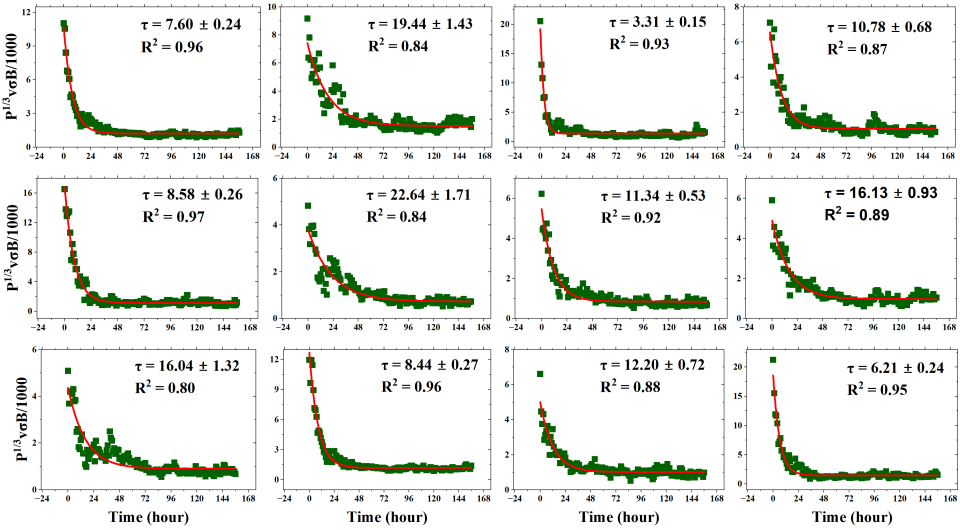


Fig. 7 Exponential fit to CF ($\rho^{\frac{1}{2}} v^{\frac{4}{3}} B$) decay profile during recovery phase on respective groups adopted from Figure 1

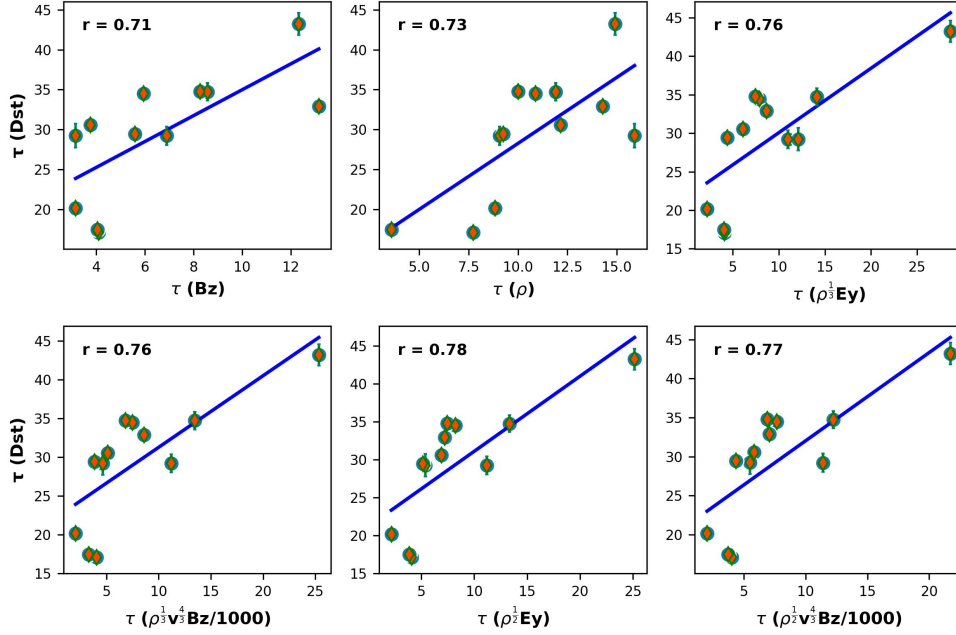


Fig. 8 The scatter error bar plots depict the relation between recovery time constant (τ) of Dst and representative IP SW parameters and their derivatives

correlated single parameters, ($\rho^{1/2}Ey$ & $\rho^{1/3}Ey$) as best-two dual parameter CFs and ($v^{4/3}Bz\rho^{1/2}/1000$ & $v^{4/3}Bz\rho^{1/3}/1000$) are taken to be best-two triple parameter CFs. With some limitation of spread in scatter plots, we can conclude that the double and triple derived CFs, which are combinations of the square root of the viscous term ($\rho^{1/2}$) and the electric field-related functions (Ey & $v^{4/3}Bz$) of ($\rho^{1/2}Ey$) and $v^{4/3}Bz\rho^{1/2}/1000$), respectively, are highly correlated with the recovery time constant of Dst. Notably, $\rho^{1/2}Ey$ is the best function to determine the recovery time characteristics of GSs as shown in Table 3.

With a Pearson's correlation coefficient of $r = 0.78$, the time constant of the dual parameter CF ($\rho^{1/2}Ey$) exhibits the highest correlation with Dst. The best-fit equation is $\tau(\text{Dst}) = (0.99 \pm 0.84)(\rho^{1/2}Ey) + (21.16 \pm 1.01)$. Overall, the results revealed significant correlations, indicating the interdependence and influence of various IP parameters/-functions on the recovery time profiles. Distinctively, combination functions of viscous term (ρ) and electric field functions such as ($\rho^{1/2}Ey$ and $v^{4/3}Bz\rho^{1/2}$) played crucial roles in determining the recovery time constant of Dst, which is an improvement to previous works by O'Brien and McPherron (2000) who have reported that, the ring current decay is best described by electric field related function vBs ($-vBz$). The rest of all

Table 3 Presents the Pearson's linear correlation coefficient and slope obtained from linear regression analyses conducted between the recovery time constants (τ) for Dst and IP SW parameters, along with their product functions. Figure 8 provide visual representations of these linear relationships for selected parameters.

No	Param.	Dst (nT)		No	Param.	Dst (nT)	
		r	s			r	s
1	B	0.04	0.09±3.06	15	$P^{\frac{1}{2}}v^{\frac{4}{3}}Bz/1000$	0.10	0.27±3.22
2	Bz	0.71	1.62±1.88	16	$P^{\frac{1}{3}}v^{\frac{4}{3}}Bz/1000$	0.72	1.08±1.45
3	σB	0.52	0.51±0.97	17	$\rho^{\frac{1}{2}}v^{\frac{4}{3}}B/1000$	0.48	0.73±1.28
4	ρ	0.73	1.65±1.23	18	$\rho^{\frac{1}{3}}v^{\frac{4}{3}}Bz/1000$	0.76	0.92±1.16
5	v	0.01	0.01±0.001	19	$\rho^{\frac{1}{2}}v^{\frac{4}{3}}Bz/1000$	0.77	1.13±1.32
6	P	0.71	1.64±1.24	20	$\rho v^{\frac{4}{3}}Bz/1000$	0.15	0.30±2.52
7	$v\sigma B/1000$	0.62	0.44±0.71	21	Ey	0.66	0.44±0.73
8	$\rho v\sigma B/1000$	0.24	0.38±1.77	22	PEy	-0.13	-0.32±3.32
9	$\rho^{\frac{1}{2}}v\sigma B/1000$	0.25	0.32±1.46	23	ρEy	0.16	0.38±2.82
10	$\rho^{\frac{1}{3}}v\sigma B/1000$	0.23	0.26±1.27	24	$\rho^{\frac{1}{2}}Ey$	0.78	0.99±1.17
11	$Pv\sigma B/1000$	0.48	1.13±2.25	25	$\rho^{\frac{1}{3}}Ey$	0.76	0.84±1.04
12	$P^{\frac{1}{2}}v\sigma B/1000$	0.35	0.62±1.79	26	$P^{\frac{1}{2}}Ey$	0.70	1.19±1.57
13	$P^{\frac{1}{3}}v\sigma B/1000$	0.29	0.40±1.49	27	$P^{\frac{1}{3}}Ey$	0.73	0.90±1.21
14	$Pv^{\frac{4}{3}}Bz/1000$	-0.14	-0.37±3.45	28	$v^{\frac{4}{3}}Bz/1000$	-0.14	-0.37±3.45

r, represents Pearson's correlation coefficient is a measure of linear relation between

$$geomagnetic\ index\ and\ other\ parameters\ (r = \frac{\Sigma(x_i - \bar{x})(y_i - \bar{y})}{\sqrt{\Sigma(x_i - \bar{x})^2 \Sigma(y_i - \bar{y})^2}})$$

s, stands for the slope of the linear regression as $y = sx + i$.

single, dual and triple parameter functions have underwent linear correlation analysis and the results are tabulated in Table 3.

3.3 Dynamical relationship between Dst and IP SW parameters during recovery phase

Based on the recovery morphology of GSs, the parabolic relationship between the Dst and IP SW parameters and derived functions has been analyzed from the result of superposed analysis. It has been determined that the recovery phase begins at the Dst minimum and lasts until the Dst reaches a quiet level. In order to accomplish this, we separately examined eight groups (r^1 , r^2 , r^3 , r^4 , entire data, CME, CIR and In as indicated in Table 1).

Figure (9 & 10) shows the scatter plots along with the second order polynomial fit between Dst and IP SW parameters and derived CFs, which were selected as the best correlated IP SW field and plasma parameters/functions. Best IP parameter/function from each class (A, B & C) as (single, double & triple) have represented as (red, green & blue filled circles) respectively, in Figures (9 & 10). The black curved lines are the best fitting parabolic curves. We have fitted our data using the second order polynomial $Y(X) = AX^2 + BX + C$. Figures (9 & 10) shows a total of eight rows (Dst-1, Dst-2, Dst-4, Dst-all, Dst-CME, Dst-CIR, Dst-3 & Int) corresponding to recovery groups

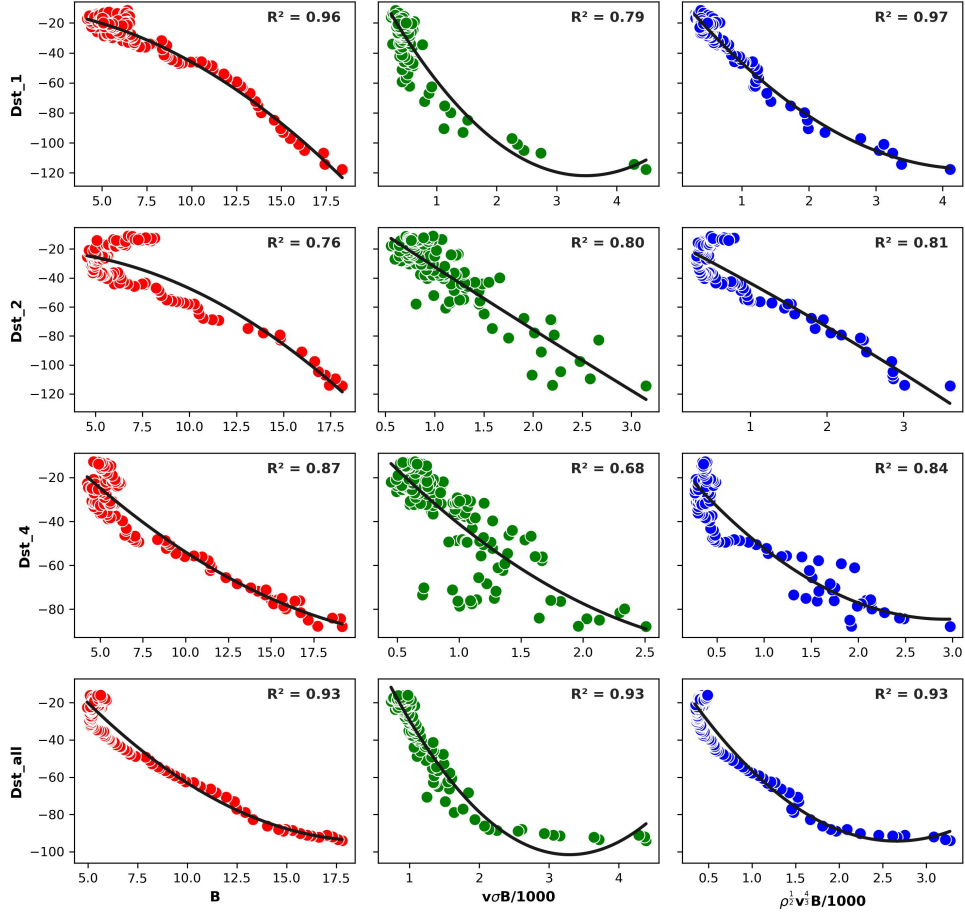


Fig. 9 The plots demonstrate the relation between Dst and some of IP SW parameters as well as derived functions based on recovery morphology of magnetic storms. The data points of the single, two, and three parameters/functions are represented by the filled circles in red, green, and blue, which correspond to the first, second, and third column panels, respectively. The black curved lines represent the most suitable parabolic curves for the data. Four groups (very-fast, fast, very-slow, whole data set, CME, CIR, and slow) are represented by four rows (Dst-1, Dst-2, Dst-4, Dst-all). Each group comprises three classes (A, B, and C) that are represented as (red, green, and blue), respectively.

(very-fast, fast, very-slow, whole data set, CME, CIR, slow and intense), respectively. The three columns (red, green, and blue) represent (single parameter, two parameter CFs, and three parameter CFs) respectively, for each of the eight recovery groups. Generally, IP SW parameters (IMF B, speed v and IMF Sigma vector σB) and derived CFs ($v\sigma B/1000$, $\rho^{1/2}v^{4/3}B/1000$) play significant role to control the recovery dynamics of geomagnetic disturbance. The combination of function $v\sigma B/1000$ with

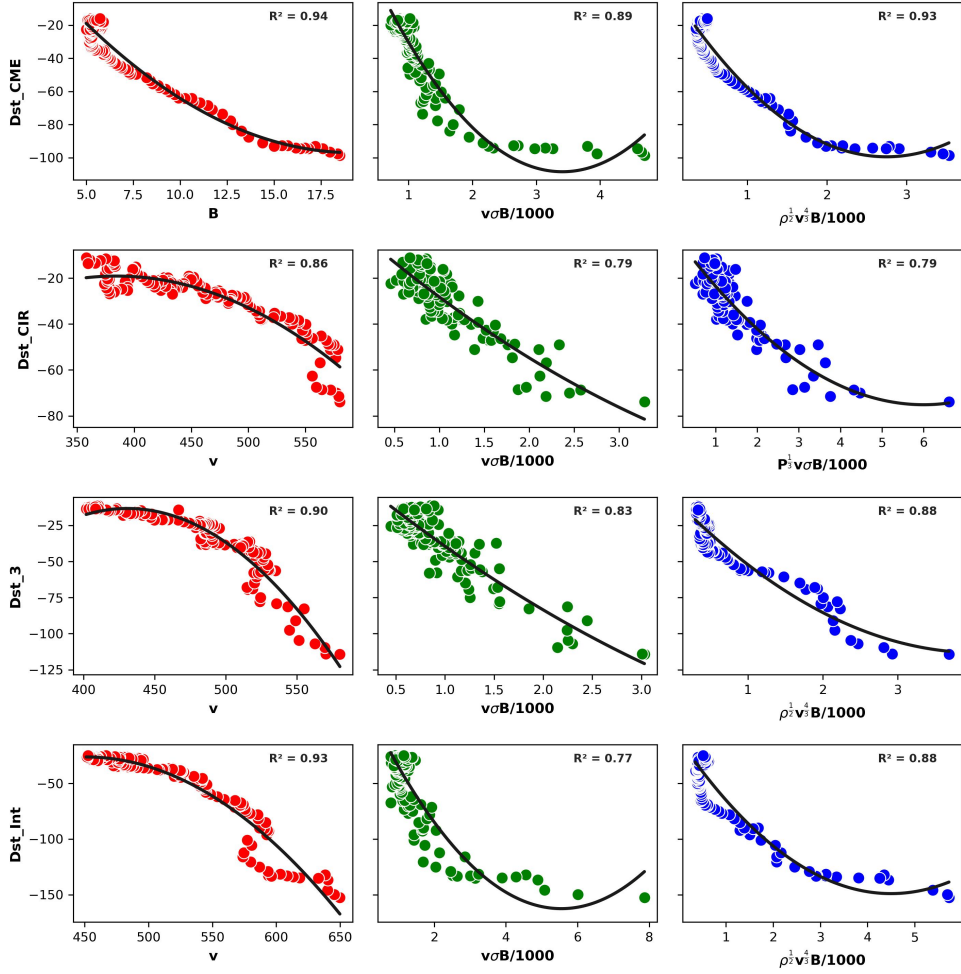


Fig. 10 The plots adopted from Figure 9, are based on four groups CME, CIR, slow and intense recovery are represented by four rows, Dst-CME, Dst-CIR, Dst-3 and Int respectively.

viscus term ρ & pressure P with power indices of $(1, \frac{1}{2}, \frac{1}{3})$ are also well representing the recovery dynamics of magnetic storms, as their coefficient of determination R^2 is tabulated in Table 4. The total IMF B correlates best for groups (r^1, r^2, r^4 , entire data set, CME) and SW speed v best correlates for groups (CIR, r^3 and Int) as a single parameter class–A. The two parameter derived CF $v\sigma B/1000$ shows the best correlation with recovery dynamics of GSs for class–B for all groups. The three parameter CFs $\rho^{\frac{1}{2}}v^{\frac{1}{3}}B/1000$ have the best correlation with storm recovery morphology for class–C, except for the CIR group, which is significantly correlated

with $P^{\frac{1}{3}}v\sigma B/1000$, implying that CIR-driven GSs are highly turbulent show high fluctuation during recovery phase. Our findings support previous research on the south-north IMF Bz fluctuations of CIR-triggered storms throughout the recovery phase (e.g. [Guarnieri et al., 2006](#); [Gupta and Badruddin, 2009](#)).

The best fit equations for the two single parameters (B & v) are $\text{Dst}(B) = -0.30B^2 - 0.64B - 9.51$ and $\text{Dst}(v) = -0.00v^2 + 3.20v - 746.24$, respectively. During the very-fast recovery group, the IMF B has the strongest relationship with Dst, with a coefficient of determination of $R^2 = 0.96$. Meanwhile, the SW velocity v has the strongest correlation with the Intense group, with a return of coefficient of determination $R^2 = 0.93$. Two parameter CF $v\sigma B/1000$ has the strongest relationship with Dst for all groups, especially, for the entire data set group with coefficient of determination $R^2 = 0.93$, with best fit equation $\text{Dst}(v\sigma B/1000) = 13.73(v\sigma B/1000)^2 - 90.42(v\sigma B/1000) + 47.29$. $\text{Dst}(\rho^{\frac{1}{2}}v^{\frac{4}{3}}B/1000) = 6.09(\rho^{\frac{1}{2}}v^{\frac{4}{3}}B/1000)^2 - 53.68(\rho^{\frac{1}{2}}v^{\frac{4}{3}}B/1000) + 1.01$ and $\text{Dst}(P^{\frac{1}{3}}v\sigma B/1000) = 2.06(P^{\frac{1}{3}}v\sigma B/1000)^2 - 24.76(P^{\frac{1}{3}}v\sigma B/1000) - 0.83$ are the best fit equations for the three-parameter SW-magnetosphere electrodynamical CFs ($\rho^{\frac{1}{2}}v^{\frac{4}{3}}B/1000$ & $P^{\frac{1}{3}}v\sigma B/1000$), respectively. With a coefficient of determination of $R^2 = 0.97$, the $\rho^{\frac{1}{2}}v^{\frac{4}{3}}B/1000$ exhibits the highest correlation with Dst during the very-fast recovery group. In the meantime, the CIR recovery group and the perturbation-related function $P^{\frac{1}{3}}v\sigma B/1000$ have a strong relationship, with a return of coefficient of determination $R^2 = 0.79$.

Overall, the three-parameter SW-magnetosphere electrodynamical CF, which combines the viscous term ($\rho^{\frac{1}{2}}$) and the electric field-related function ($v^{\frac{4}{3}}B/1000$) ($\rho^{\frac{1}{2}}v^{\frac{4}{3}}B/1000$), significantly impacts the recovery phase morphology of geomagnetic disturbances.

4 Summary and Conclusions

In the present study, geomagnetic index Dst, IP SW plasma and field parameters, and derived CFs for 1-hour averaged resolution have been retrieved. The study focused on analyzing the recovery characteristics of GSs by examining 57 events with $\text{Dst} \leq 50$ nT. Most of the analyzed events are triggered by CMEs and small amount of events driven by CIRs. For both storms driven by CMEs and CIRs, we fitted exponential curves during the recovery phase. We may conclude from these results that the ring current decays faster for storms with short main phase durations in general, and it decays quickly for one day followed by gradual long-lasting second-step recovery. Magnetic storms with longer main phase duration, on the other hand, exhibit one step slow and gradual recovery. Storms with shorter main and recovery phases show two-step recovery where as storms long lasting main and recovery durations show one step sluggish recovery. Only, intense geomagnetic disturbances show two-step recovery. During recovery of very intense storms ($\text{Dst} \leq -150$ nT) only the first initial phase (28%) of recovery period has perturbed. Notably, intense storms fluctuates for short time and moderate storms continue their recovery with turbulence for longer periods.

We used linear correlation analysis for the recorded recovery time constants between Dst and IP SW parameters/functions to get the best parameter which represent the

Table 4 Presents the results of correlation obtained from second order polynomial fits conducted between the Dst and IP SW parameters, along with their products for eight groups. The coefficient of determination R^2 were determined based on the recovery profiles or morphologies.

No	Param.	Groups							
		all	r^1	r^2	r^3	r^4	CME	CIR	Int
1	B	0.921 ^{β}	0.96	0.76	0.85	0.87	0.94	0.73	0.92
2	Bz	0.35	0.57	0.61	0.50	0.53	0.45	0.24	0.34
3	σ B	0.90	0.63	0.70	0.79	0.74	0.86	0.65	0.78
4	ρ	0.57	0.41	0.52	0.58	0.63	0.53	0.68	0.53
5	v	0.85	0.93	0.67	0.90	0.83	0.90	0.86	0.925 ^{β}
6	P	0.84	0.78	0.61	0.80	0.75	0.82	0.65	0.81
7	$v\sigma$ B/1000	0.924 ^{β}	0.79	0.80	0.83	0.68	0.89	0.79	0.77
8	$\rho v\sigma$ B/1000	0.81	0.69	0.68	0.77	0.79	0.77	0.69	0.75
9	$\rho^{\frac{1}{2}}v\sigma$ B/1000	0.86	0.73	0.74	0.83	0.83	0.82	0.71	0.79
10	$\rho^{\frac{1}{3}}v\sigma$ B/1000	0.88	0.75	0.76	0.84	0.82	0.84	0.71	0.81
11	$Pv\sigma$ B/1000	0.75	0.67	0.78	0.82	0.80	0.71	0.73	0.64
12	$P^{\frac{1}{2}}v\sigma$ B/1000	0.86	0.74	0.80	0.87	0.80	0.82	0.79	0.73
13	$P^{\frac{1}{3}}v\sigma$ B/1000	0.86	0.75	0.81	0.87	0.82	0.85	0.80	0.75
14	$Pv^{\frac{4}{3}}Bz$ /1000	0.30	0.29	0.22	0.45	0.09	0.26	0.16	0.31
15	$P^{\frac{1}{2}}v^{\frac{4}{3}}Bz$ /1000	0.37	0.39	0.55	0.40	0.19	0.33	0.32	0.32
16	$P^{\frac{1}{3}}v^{\frac{4}{3}}Bz$ /1000	0.37	0.39	0.63	0.38	0.24	0.34	0.32	0.29
17	$\rho^{\frac{1}{2}}v^{\frac{4}{3}}B$ /1000	0.927 ^{β}	0.97	0.81	0.88	0.84	0.93	0.66	0.88
18	$\rho^{\frac{1}{3}}v^{\frac{4}{3}}Bz$ /1000	0.43	0.44	0.69	0.48	0.35	0.40	0.31	0.37
19	$\rho^{\frac{1}{2}}v^{\frac{4}{3}}Bz$ /1000	0.44	0.45	0.71	0.51	0.34	0.40	0.32	0.41
20	$\rho v^{\frac{4}{3}}Bz$ /1000	0.42	0.33	0.67	0.58	0.09	0.36	0.43	0.41
21	Ey	0.40	0.51	0.57	0.43	0.38	0.37	0.26	0.22
22	ρ Ey	0.45	0.36	0.70	0.58	0.09	0.38	0.44	0.42
23	$\rho^{\frac{1}{2}}$ Ey	0.46	0.47	0.72	0.53	0.40	0.42	0.32	0.42
24	$\rho^{\frac{1}{3}}$ Ey	0.44	0.51	0.70	0.51	0.40	0.42	0.30	0.39
25	PEy	0.31	0.28	0.25	0.48	0.10	0.27	0.16	0.32
26	$P^{\frac{1}{2}}$ Ey	0.39	0.41	0.60	0.43	0.23	0.35	0.32	0.34
27	$P^{\frac{1}{3}}$ Ey	0.40	0.42	0.66	0.42	0.29	0.37	0.31	0.32
28	$v^{\frac{4}{3}}Bz$ /1000	0.35	0.50	0.66	0.38	0.33	0.33	0.26	0.19

To obtain the ideal parameter, ^{β} indicate the values to the third decimal place.

recovery time of magnetic storms. The decay rate of geomagnetic disturbances, as observed through the Dst index, could be best described by the decay rates of the function ($\rho^{\frac{1}{2}}$ Ey) with the corresponding Pearson correlation coefficient 0.791, where both viscous term (ρ) and the dawn-dusk electric field (Ey) contribute to determine the recovery rate of geomagnetic disturbances. Earlier works suggested that the ring current decay is best described by electric field related function [v Bs ($-v$ Bz) or Ey]. Our analysis suggests that, this electric field related function when coupled with a viscous function ($\rho^{\frac{1}{2}}$) (i.e. $\rho^{\frac{1}{2}}$ Ey) better describe the ring current decay compared to electric field related function Ey ($-Bz$) alone.

The recovery phase morphology demonstrates a highly significant dynamic relationship between Dst and IP SW parameters/functions. IP SW parameters (IMF B, speed

v and IMF Sigma vector σB) and derived CFs ($v\sigma B$, $\rho^{\frac{1}{2}}v^{\frac{4}{3}}B$) plays significant role to control the recovery dynamics of geomagnetic disturbance. The recovery morphology of geomagnetic disturbances is strongly correlated with (IMF B, CF $v\sigma B$, $\rho^{\frac{1}{2}}v^{\frac{4}{3}}B$) in Classes (A, B, & C, see Section 3.1) as (single, two parameter CF, three parameter CF), respectively.

These findings contribute to our understanding of how SW controls the ring current decay during geomagnetic disturbances. The decay rate of CF, which includes the viscous term ρ and the electric field function ($\rho^{\frac{1}{2}}Ey$), appears to show a significant impact on the recovery rate of Dst, implying to be an important factor impacting the the ring current decay rate. On the other hand, the three-parameter SW-magnetosphere electrodynamical CF, which combines the viscous term ($\rho^{\frac{1}{2}}$) and the electric field-related function ($v^{\frac{4}{3}}B/1000$) ($\rho^{\frac{1}{2}}v^{\frac{4}{3}}B/1000$), significantly impacts the recovery phase morphology of geomagnetic disturbances. Overall, this study enhances our knowledge of the recovery dynamics of magnetic storms and their relationship with various geomagnetic and interplanetary parameters, providing valuable insights into the complex processes involved in geomagnetic storm recovery. Since the recovery phase of GS is nonlinear, and recovery process is complex, this work instigates and contributes towards this concern. However, it is desirable to continue the efforts towards better understanding of the mechanisms and processes during recovery of geomagnetic disturbances.

Author contributions. OA planned the study, wrote manuscript, and participated in the data analysis. BB contributed to design the approach, review and editing. MD took part in the interpretation, review and editing process.

Data Availability. Analyzed data were extracted from NASA/OMNIWeb, available on <http://omniweb.gsfc.nasa.gov>.

Competing interests. The authors declare no competing interests.

Acknowledgements. This study used data obtained from the GSFC/SPDF OMNI-Web interface, which can be found at <https://omniweb.gsfc.nasa.gov>. We would like to thank the reviewers for their insightful feedback and constructive suggestions, which considerably improved the quality of this work.

References

- Aguado, J., Cid, C., Cerrato, Y., Saiz, E.: Magnetosphere behaviour during the recovery phase of geomagnetic storms. *Lecture Notes and Essays in Astrophysics III* **3**, 127 (2014)
- Aguado, J., Cid, C., Saiz, E., Cerrato, Y.: A hyperbolic decay of the dst index during the recovery phase of intense geomagnetic storms. *arXiv: Earth and Planetary Astrophysics* (2010)
- Akasofu, S.-I.: Prediction of development of geomagnetic storms using the solar wind-magnetosphere energy coupling function epsilon. *planss* **29**(11), 1151–1158 (1981) [https://doi.org/10.1016/0032-0633\(81\)90121-5](https://doi.org/10.1016/0032-0633(81)90121-5)

- Ahmed, O.M., Zaheer Ahmad, B., Derouich, M.: Characteristics and development of the main phase disturbance in geomagnetic storms ($Dst \leq -50$ nT). arXiv e-prints, 2402–03261 (2024) <https://doi.org/10.48550/arXiv.2402.03261> arXiv:2402.03261 [astro-ph.SR]
- Badruddin: Interplanetary shocks, magnetic clouds, stream interfaces and resulting geomagnetic disturbances. *Planetary and Space Science* **46**, 1015–1028 (1998)
- Badruddin, Aslam, O.P.M., Derouich, M.: Study of the recovery characteristics of intense cosmic-ray decreases. *Astrophys. Space Sci.* **366**, 62 (2021) <https://doi.org/10.10072Fs10509-021-03968-w>
- Bergin, A., Chapman, S.C., Watkins, N.W., Moloney, N.R., Gjerloev, J.W.: Extreme Event Statistics in Dst, SYM-H, and SMR Geomagnetic Indices. *Space Weather* **21**(3), 2022–003304 (2023) <https://doi.org/10.1029/2022SW003304>
- Borovsky, J.E., Denton, M.H.: Differences between CME-driven storms and CIR-driven storms. *Journal of Geophysical Research (Space Physics)* **111**(A7), 07–08 (2006) <https://doi.org/10.1029/2005JA011447>
- Badruddin, A., Falak, Z.: Study of the geoeffectiveness of coronal mass ejections, corotating interaction regions and their associated structures observed during Solar Cycle 23. *Astrophys. Space Sci.* **361**(8), 253 (2016) <https://doi.org/10.1007/s10509-016-2839-4>
- Burton, R.K., McPherron, R.L., Russell, C.T.: An empirical relationship between interplanetary conditions and Dst. *J. Geophys. Res.* **80**(31), 4204 (1975) <https://doi.org/10.1029/JA080i031p04204>
- Bothmer, V., Schwenn, R.: The interplanetary and solar causes of major geomagnetic storms. *Journal of geomagnetism and geoelectricity* **47**, 1127–1132 (1995)
- Badruddin, Singh, Y.P.: Geoeffectiveness of magnetic cloud, shock/sheath, interaction region, high-speed stream and their combined occurrence. *Planetary and Space Science* **57**, 318–331 (2009)
- Boroyev, R.N., Vasiliev, M.S.: The auroral activity during the main phase of magnetic storms. *Advances in Space Research* **71**(1), 1137–1145 (2023) <https://doi.org/10.1016/j.asr.2022.10.034>
- Carrillo-Vargas, A., Pérez-Enríquez, R., López-Montes, R., Rodríguez-Martínez, M., Ugalde-Calvillo, L.G.: Radio signal anomalies detected with MEXART in 2012 during the recovery phase of geomagnetic storms. *Advances in Space Research* **58**(10), 2057–2066 (2016) <https://doi.org/10.1016/j.asr.2016.05.014>
- Cid, C., Palacios, J., Saiz, E., Guerrero, A., Cerrato, Y.: On extreme geomagnetic storms. *Journal of Space Weather and Space Climate* **4** (2014)

- Cane, H.V., Richardson, I.G.: Interplanetary coronal mass ejections in the near-Earth solar wind during 1996-2002. *Journal of Geophysical Research (Space Physics)* **108**(A4), 1156 (2003) <https://doi.org/10.1029/2002JA009817>
- Choraghe, K., Raghav, A., Chakrabarty, D., Kasthurirangan, S., Bijewar, N.: Properties of the Recovery Phase of Extreme Storms. *Journal of Geophysical Research (Space Physics)* **126**(9), 28685 (2021) <https://doi.org/10.1029/2020JA028685>
- Daglis, I.A.: The role of magnetosphere-ionosphere coupling in magnetic storm dynamics. Washington DC American Geophysical Union Geophysical Monograph Series **98**, 107–116 (1997) <https://doi.org/10.1029/GM098p0107>
- Dasso, S., Gómez, D., Mandrini, C.H.: Ring current decay rates of magnetic storms: A statistical study from 1957 to 1998. *Journal of Geophysical Research (Space Physics)* **107**(A5), 1059 (2002) <https://doi.org/10.1029/2000JA000430>
- Denton, M.H., Thomsen, M.F., Reeves, G.D., Larsen, B.A., Henderson, M.G., Jordanova, V.K., Fernandes, P.A., Friedel, R.H.W., Skoug, R.M., Funsten, H.O., MacDonald, E.A., Spence, H.A.: The Evolution of the Plasma Sheet Ion Composition: Storms and Recoveries. *Journal of Geophysical Research: Space Physics* **122**(12), 12040–12054 (2017) <https://doi.org/10.1002/2017JA024475>
- Echer, E., Gonzalez, W.D., Tsurutani, B.T., Gonzalez, A.L.C.: Interplanetary conditions causing intense geomagnetic storms (Dst \leq -100 nT) during solar cycle 23 (1996-2006). *Journal of Geophysical Research (Space Physics)* **113**(A5), 05221 (2008) <https://doi.org/10.1029/2007JA012744>
- Fenrich, F.R., Luhmann, J.G.: Geomagnetic response to magnetic clouds of different polarity. *Geophys. Res. Lett.* **25**(15), 2999–3002 (1998) <https://doi.org/10.1029/98GL51180>
- Gupta, V., Badruddin: Interplanetary structures and solar wind behaviour during major geomagnetic perturbations. *Journal of Atmospheric and Solar-Terrestrial Physics* **71**(8-9), 885–896 (2009) <https://doi.org/10.1016/j.jastp.2009.02.004>
- Garrett, H.B., Dessler, A.J., Hill, T.W.: Influence of solar wind variability on geomagnetic activity. *Journal of Geophysical Research* **79**, 4603–4610 (1974)
- Gonzalez, W.D., Joselyn, J.A., Kamide, Y., Kroehl, H.W., Rostoker, G., Tsurutani, B.T., Vasyliunas, V.M.: What is a geomagnetic storm? *J. Geophys. Res.* **99**(A4), 5771–5792 (1994) <https://doi.org/10.1029/93JA02867>
- Gopalswamy, N.: Solar connections of geoeffective magnetic structures. *Journal of Atmospheric and Solar-Terrestrial Physics* **70**(17), 2078–2100 (2008) <https://doi.org/10.1016/j.jastp.2008.06.010>
- Gosling, J., Pizzo, V.J.: Formation and evolution of corotating interaction regions and

- their three dimensional structure. *Space Science Reviews* **89**, 21–52 (1999)
- Gonzalez, W.D., Tsurutani, B.T., Clúa de Gonzalez, A.L.: Interplanetary origin of geomagnetic storms. *Space Sci. Rev.* **88**, 529–562 (1999) <https://doi.org/10.1023/A:1005160129098>
- Gonzalez, W.D., Tsurutani, B.T., Gonzalez, A.L.C., Smith, E.J., Tang, F., Akasofu, S.-I.: Solar wind-magnetosphere coupling during intense magnetic storms (1978-1979). *J. Geophys. Res.* **94**(A7), 8835–8851 (1989) <https://doi.org/10.1029/JA094iA07p08835>
- Guarnieri, F.L., Tsurutani, B.T., Gonzalez, W.D., Gonzalez, A.L.C., Grande, M., Soraas, F., Ech, E.: ICME and CIR storms with particular emphasis on HILDCAA events. In: Gopalswamy, N., Bhattacharyya, A. (eds.) *Proceedings of the ILWS Workshop*, p. 266 (2006)
- Gopalswamy, N., Yashiro, S., Akiyama, S., Xie, H., Mäkelä, P., Fok, M.-C., Ferradas, C.P.: What Is Unusual About the Third Largest Geomagnetic Storm of Solar Cycle 24? *Journal of Geophysical Research (Space Physics)* **127**(8), 30404 (2022) <https://doi.org/10.1029/2022JA030404> [arXiv:2207.11630](https://arxiv.org/abs/2207.11630) [astro-ph.SR]
- Hamilton, D.C., Gloeckler, G., Ipavich, F.M., Stüdemann, W., Wilken, B., Kremser, G.: Ring current development during the great geomagnetic storm of February 1986. *J. Geophys. Res.* **93**(A12), 14343–14355 (1988) <https://doi.org/10.1029/JA093iA12p14343>
- Jian, L.K., Russell, C.T., Luhmann, J.G., Skoug, R.M., Steinberg, J.T.: Stream Interactions and Interplanetary Coronal Mass Ejections at 5.3 AU near the Solar Ecliptic Plane. *Sol. Phys.* **250**(2), 375–402 (2008) <https://doi.org/10.1007/s11207-008-9204-x>
- Ji, Y., Shen, C.: The loss rates of O^+ in the inner magnetosphere caused by both magnetic field line curvature scattering and charge exchange reactions. *Physics of Plasmas* **21**(3), 032903 (2014) <https://doi.org/10.1063/1.4868863>
- Kane, R.P.: How good is the relationship of solar and interplanetary plasma parameters with geomagnetic storms. *Journal of Geophysical Research* **110** (2005)
- Kane, R.P., Echer, E.: Phase shift (time) between storm-time maximum negative excursions of geomagnetic disturbance index *dst* and interplanetary *bz*. *Journal of Atmospheric and Solar-Terrestrial Physics* **69**, 1009–1020 (2007)
- Khabarova, O.V., Yermolaev, Y.I.: Solar wind parameters' behavior before and after magnetic storms. *Journal of Atmospheric and Solar-Terrestrial Physics* **70**, 384–390 (2008)
- Liemohn, M.W., Ganushkina, N.Y., Ilie, R., Welling, D.T.: Challenges associated with

- near-earth nightside current. *Journal of Geophysical Research: Space Physics* **121**, 6763–6768 (2016)
- Lin, J.-W.: Geomagnetic Storm Related to Disturbance Storm Time Indices: Geomagnetic Storm. *European Journal of Environment and Earth Sciences* **2**(6), 1–3 (2021) <https://doi.org/10.24018/ejgeo.2021.2.6.199>
- Liemohn, M.W., Kozyra, J.U., Jordanova, V.K., Khazanov, G.V., Thomsen, M.F., Cayton, T.E.: Analysis of early phase ring current recovery mechanisms during geomagnetic storms. *Geophys. Res. Lett.* **26**(18), 2845–2848 (1999) <https://doi.org/10.1029/1999GL900611>
- Lakhina, G., Tsurutani, B.: Supergeomagnetic Storms: Past, Present, and Future, pp. 157–185 (2018). <https://doi.org/10.1016/B978-0-12-812700-1.00007-8>
- Mansilla, G.A.: Solar wind and IMF parameters associated with geomagnetic storms with Dst 50 nT. *physscr* **78**(4), 045902 (2008) <https://doi.org/10.1088/0031-8949/78/04/045902>
- Mayaud, P.N.: Derivation, meaning, and use of geomagnetic indices. *Geophysical monograph* **22**, 607 (1980)
- Mustajab, F., Badruddin: Geoeffectiveness of the interplanetary manifestations of coronal mass ejections and solar-wind stream-stream interactions. *Astrophys. Space Sci.* **331**(1), 91–104 (2011) <https://doi.org/10.1007/s10509-010-0428-5>
- Manu, V., Balan, N., Zhang, Q.-H., Xing, Z.-Y.: Double Superposed Epoch Analysis of Geomagnetic Storms and Corresponding Solar Wind and IMF in Solar Cycles 23 and 24. *Space Weather* **21**(3), 2022–003314 (2023) <https://doi.org/10.1029/2022SW003314>
- Monreal MacMahon, R., Llop-Romero, C.: Ring current decay time model during geomagnetic storms: a simple analytical approach. *Annales Geophysicae* **26**(9), 2543–2550 (2008) <https://doi.org/10.5194/angeo-26-2543-2008>
- Monreal MacMahon, R., Llop-Romero, C.: A two-step ring current decay time model during the passive recovery phase of magnetic storms. *Journal of Atmospheric and Solar-Terrestrial Physics* **73**, 1831–1839 (2011) <https://doi.org/10.1016/j.jastp.2011.04.007> [arXiv:1104.007](https://arxiv.org/abs/1104.007) [astro-ph.SR]
- Miteva, R., Samwel, S.W.: Catalog of Geomagnetic Storms with Dst Index ≤ -50 nT and Their Solar and Interplanetary Origin (1996–2019). *Atmosphere* **14**(12), 1744 (2023) <https://doi.org/10.3390/atmos14121744>
- Nuraeni, F., Ruhimat, M., Aris, M.A., Ratnasari, E.A., Purnomo, C.: Development of 24 hours Dst index prediction from solar wind data and IMF Bz using NARX. In: *Journal of Physics Conference Series*. *Journal of Physics Conference Series*, vol.

- 2214, p. 012024 (2022). <https://doi.org/10.1088/1742-6596/2214/1/012024>
- Newell, P.T., Sotirelis, T., Liou, K., Meng, C.-I., Rich, F.J.: A nearly universal solar wind-magnetosphere coupling function inferred from 10 magnetospheric state variables. *Journal of Geophysical Research (Space Physics)* **112**(A1), 01206 (2007) <https://doi.org/10.1029/2006JA012015>
- Newell, P.T., Sotirelis, T., Liou, K., Rich, F.J.: Pairs of solar wind-magnetosphere coupling functions: Combining a merging term with a viscous term works best. *Journal of Geophysical Research (Space Physics)* **113**(A4), 04218 (2008) <https://doi.org/10.1029/2007JA012825>
- O'Brien, T.P., McPherron, R.L.: An empirical phase space analysis of ring current dynamics: Solar wind control of injection and decay. *Journal of Geophysical Research* **105**, 7707–7719 (2000)
- Pick, L., Effenberger, F., Zhelavskaya, I., Korte, M.: A Statistical Classifier for Historical Geomagnetic Storm Drivers Derived Solely From Ground-Based Magnetic Field Measurements. *Earth and Space Science* **6**(10), 2000–2015 (2019) <https://doi.org/10.1029/2019EA000726>
- Patari, A., Guha, A.: Comparative study on the effects of CME and CIR-induced geomagnetic storms on the ionosphere of northern and southern hemispheric regions during the different phases of solar cycle 24. *Advances in Space Research* **71**(12), 5147–5170 (2023) <https://doi.org/10.1016/j.asr.2023.02.010>
- Rawat, R., Alex, S., Lakhina, G.S.: Storm-time characteristics of intense geomagnetic storms ($Dst \leq -200$ nT) at low-latitudes and associated energetics. *Journal of Atmospheric and Solar-Terrestrial Physics* **72**(18), 1364–1371 (2010) <https://doi.org/10.1016/j.jastp.2010.09.029>
- Richardson, I.G., Cane, H.V.: Solar wind drivers of geomagnetic storms during more than four solar cycles. *Journal of Space Weather and Space Climate* **2**, 01 (2012) <https://doi.org/10.1051/swsc/2012001>
- Raghav, A.N., Choraghe, K., Shaikh, Z.I.: The cause of an extended recovery from an ICME-induced extreme geomagnetic storm: a case study. *Mon. Not. R. Astron. Soc.* **488**(1), 910–917 (2019) <https://doi.org/10.1093/mnras/stz1608>
- Raghav, A.N., Kule, A., Bhaskar, A., Mishra, W., Vichare, G., Surve, S.: Torsional Alfvén Wave Embedded ICME Magnetic Cloud and Corresponding Geomagnetic Storm. *Astrophys. J.* **860**(1), 26 (2018) <https://doi.org/10.3847/1538-4357/aabba3> [arXiv:1810.06013](https://arxiv.org/abs/1810.06013) [physics.space-ph]
- Richardson, I.G., Webb, D.F., Zhang, J., Berdichevsky, D., Biesecker, D.A., Kasper, J.C., Kataoka, R., Steinberg, J.T., Thompson, B.J., Wu, C.-C., Zhukov, A.N.: Correction to “major geomagnetic storms ($dst < -100$ nt) generated by corotating

- interaction regions". *Journal of Geophysical Research* **112** (2007)
- Saba, M.M.F., Gonzalez, W.D., Gonzalez, A.L.C.: Relationships between the ae, ap and dst indices near solar minimum (1974) and at solar maximum (1979). *Annales Geophysicae* **15**, 1265–1270 (1997)
- Shaikh, Z.I., Raghav, A., Vichare, G., Bhaskar, A., Mishra, W., Choraghe, K.: Concurrent effect of Alfvén waves and planar magnetic structure on geomagnetic storms. *Mon. Not. R. Astron. Soc.* **490**(3), 3440–3447 (2019) <https://doi.org/10.1093/mnras/stz2806>
- Singh, Y.P., Singh, M., Badruddin: Analysis of plasma and field conditions during some intensely geo-effective transient solar/interplanetary disturbances of solar cycle 23. *Journal of Astrophysics and Astronomy* **27**, 361–366 (2006)
- Srivastava, N., Venkatakrisnan, P.: Solar and interplanetary sources of major geomagnetic storms during 1996–2002. *Journal of Geophysical Research* **109** (2004)
- Telloni, D., D’Amicis, R., Bruno, R., Perrone, D., Sorriso-Valvo, L., Raghav, A.N., Choraghe, K.: Alfvénicity-related long recovery phases of geomagnetic storms: A space weather perspective. *The Astrophysical Journal* **916**(2), 64 (2021) <https://doi.org/10.3847/1538-4357/ac071f>
- Tsurutani, B.T., Gonzalez, W.D.: The Interplanetary causes of magnetic storms: A review. Washington DC American Geophysical Union Geophysical Monograph Series **98**, 77–89 (1997) <https://doi.org/10.1029/GM098p0077>
- Tsurutani, B.T., Gonzalez, W.D., Gonzalez, A.L.C., Guarnieri, F.L., Gopalswamy, N., Grande, M., Kamide, Y., Kasahara, Y., Lu, G., Mann, I., McPherron, R., Soraas, F., Vasyliunas, V.: Corotating solar wind streams and recurrent geomagnetic activity: A review. *Journal of Geophysical Research (Space Physics)* **111**(A7), 07–01 (2006) <https://doi.org/10.1029/2005JA011273>
- Tsurutani, B.T., Gonzalez, W.D., Tang, F.M., Lee, Y.T.: Great magnetic storms. *Geophysical Research Letters* **19**, 73–76 (1992)
- Takahashi, S., Iyemori, T., Takeda, M.: A simulation of the storm-time ring current. *planss* **38**(9), 1133–1141 (1990) [https://doi.org/10.1016/0032-0633\(90\)90021-H](https://doi.org/10.1016/0032-0633(90)90021-H)
- Vallat, C., Dandouras, I., Dunlop, M.W., Balogh, A., Lucek, E.A., Parks, G.K., Wilber, M.Q., Roelof, E.C., Chanteur, G.M., Rème, H.: First current density measurements in the ring current region using simultaneous multi-spacecraft cluster-fgm data. *Annales Geophysicae* **23**, 1849–1865 (2005)
- Webb, D.F., Howard, T.A.: Coronal Mass Ejections: Observations. *Living Reviews in Solar Physics* **9**(1), 3 (2012) <https://doi.org/10.12942/lrsp-2012-3>

- Wang, Y., Ye, P., Wang, S., Zhou, G., Wang, J.T.: A statistical study on the geoeffectiveness of earth-directed coronal mass ejections from march 1997 to december 2000. *Journal of Geophysical Research* **107**, 1340 (2002)
- Xie, H., Gopalswamy, N., Manoharan, P.K., Lara, A., Yashiro, S., Lepri, S.: Long-lived geomagnetic storms and coronal mass ejections. *Journal of Geophysical Research (Space Physics)* **111**(A1), 01103 (2006) <https://doi.org/10.1029/2005JA011287>
- YACOB, A.: Decay rate of recovery phase of geomagnetic storms and dissipation of associated ring currents. *MAUSAM* **15**(4), 579–594 (1964) <https://doi.org/10.54302/mausam.v15i4.5576>
- Yan, Z., Chao, Y.: Ring current dynamics in the earth’s inner magnetosphere. *Reviews of Geophysics and Planetary Physics* **53**(5), 556–566 (2022)
- Yermolaev, Y.I., Lodkina, I.G., Dremukhina, L.A., Yermolaev, M.Y., Khokhlachev, A.A.: What Solar–Terrestrial Link Researchers Should Know about Interplanetary Drivers. *Universe* **7**(5), 138 (2021) <https://doi.org/10.3390/universe7050138> [arXiv:2002.09415](https://arxiv.org/abs/2002.09415) [physics.space-ph]
- Yermolaev, Y.I., Lodkina, I.G., Nikolaeva, N.S., Yermolaev, M.Y.: Recovery phase of magnetic storms induced by different interplanetary drivers. *Journal of Geophysical Research (Space Physics)* **117**(A8), 08207 (2012) <https://doi.org/10.1029/2012JA017716> [arXiv:1111.6914](https://arxiv.org/abs/1111.6914) [physics.space-ph]
- Yermolaev, Y.I., Lodkina, I.G., Nikolaeva, N.S., Yermolaev, M.Y.: Influence of the interplanetary driver type on the durations of the main and recovery phases of magnetic storms. *Journal of Geophysical Research (Space Physics)* **119**(10), 8126–8136 (2014) <https://doi.org/10.1002/2014JA019826> [arXiv:1312.7787](https://arxiv.org/abs/1312.7787) [physics.space-ph]
- Zhang, J., Richardson, I.G., Webb, D.F., Gopalswamy, N., Huttunen, E., Kasper, J.C., Nitta, N.V., Poomvises, W., Thompson, B.J., Wu, C.-C., Yashiro, S., Zhukov, A.N.: Solar and interplanetary sources of major geomagnetic storms (Dst \leq -100 nT) during 1996-2005. *Journal of Geophysical Research (Space Physics)* **112**(A10), 10102 (2007) <https://doi.org/10.1029/2007JA012321>